UNCLASSIFIED

TM No.
TC-179-71

NAVAL UNDERWATER SYSTEMS CENTER

Technical Memorandum

RECEIVER OPERATING CHARACTERISTICS FOR PHASE-INCOHERENT DETECTION OF MULTIPLE OBSERVATIONS

28 September 1971

Prepared by: Albert H. Nuttall
Albert H. Nuttall
Office of Director of
Science and Technology

Robert Garber
Robert Garber
Submarine Sonar Dept.

This report expresses the views of the authors and not necessarily those of the Center. It represents Center policy only when accompanied by an official letter of endorsement.

Approved for public release; distribution unlimited.

UNCLASSIFIED

Report Documentation Page

Form Approved
OMB No. 0704-0188

1. REPORT DATE	2. REPORT TYPE	3. DATES COVERED
28 SEP 1971	**Technical Memorandum**	**28-09-1971 to 28-09-1971**

4. TITLE AND SUBTITLE	5a. CONTRACT NUMBER
Receiver Operating Characteristics for Phase-Incoherent Detection of Multiple Observations	5b. GRANT NUMBER
	5c. PROGRAM ELEMENT NUMBER
6. AUTHOR(S) **Albert Nuttall; Robert Garber**	5d. PROJECT NUMBER **A75205**
	5e. TASK NUMBER
	5f. WORK UNIT NUMBER
7. PERFORMING ORGANIZATION NAME(S) AND ADDRESS(ES) **Naval Undersea Warfare Center, Division Newport,1176 Howell Street,Newport,RI,02841-1708**	8. PERFORMING ORGANIZATION REPORT NUMBER **TC-179-71**
9. SPONSORING/MONITORING AGENCY NAME(S) AND ADDRESS(ES) **Chief of Naval Material**	10. SPONSOR/MONITOR'S ACRONYM(S)
	11. SPONSOR/MONITOR'S REPORT NUMBER(S)

12. DISTRIBUTION/AVAILABILITY STATEMENT
Approved for public release; distribution unlimited

13. SUPPLEMENTARY NOTES
NUWC2015

14. ABSTRACT
Receiver operating characteristics for phase-incoherent detection of M multiple observations ore presented, for a wide range of values of M and signal-to-noise ratio. Comparison with a processor capable of coherently summing up all M signal components is made. The additional signal-to-noise ratio required for the phase-incoherent combiner is found to be greater?? at the lower false-alarm and detection probabilities.

15. SUBJECT TERMS
Sonar Signal Processing; M signal

16. SECURITY CLASSIFICATION OF:			17. LIMITATION OF ABSTRACT	18. NUMBER OF PAGES	19a. NAME OF RESPONSIBLE PERSON
a. REPORT **unclassified**	b. ABSTRACT **unclassified**	c. THIS PAGE **unclassified**	**Same as Report (SAR)**	**58**	

TM No.
TC-179-71

NAVAL UNDERWATER SYSTEMS CENTER
Newport, Rhode Island 02840

ABSTRACT

Receiver operating characteristics for phase-incoherent detection of M multiple observations are presented, for a wide range of values of M and signal-to-noise ratio. Comparison with a processor capable of coherently summing up all M signal components is made. The additional signal-to-noise ratio required for the phase-incoherent combiner is found to be greater at the lower false-alarm and detection probabilities.

ADMINISTRATIVE INFORMATION

This memorandum was prepared under Project No. A75205, Sub-Project No. ZFXX212001, "Statistical Communication with Applications to Sonar Signal Processing," Principal Investigator Dr. A. H. Nuttall, Code TC. The sponsoring activity is Chief of Naval Material, Program Manager Dr. J. H. Huth.

The authors of this memorandum are located at the New London Laboratory and may be addressed via Officer in Charge, New London Laboratory, Naval Underwater Systems Center, New London, Connecticut 06320.

INTRODUCTION

In many cases, received signals contain multiple (M-ary) replicas of the signal information at predictable locations in the time and/or frequency domain. Knowledge of the signal replicas can be obtained by analysis in a noise-free, or low noise environment, by placing measurement transducers at positions closer than is practical under normal operating conditions, or by utilizing artificial means to force higher signal levels than are usually available. Once these multiple features of the signal are known, they can be utilized to enhance the detection capability of a system operating on them. However, the complexity of any system that attempts to detect by use of multiple signal characteristics will be increased.

This memorandum examines the gain available when phase-coherent vs. phase-incoherent detection is used, as a function of the number M of signal characteristics and the allowable false alarm probability. It is intended to supply the information required to make the tradeoff between increased detection capability and system complexity.

The analytical results in this memorandum are not new; for example, Helstrom [Ref. 1, Ch. VI] presents all the equations required. However, there is inadequate quantitative evaluation of the M-ary phase-incoherent processor (Ref. 1 contains one figure on page 181 for a false alarm probability of 10^{-10}). Thus, comparison with an ideal processor is not possible for a significant range of signal-to-noise ratios, values of M, and false-alarm probabilities. The present results rectify this situation and make the comparison. The method of computation of the operating characteristics is given in Refs. 2 and 3.

PROBLEM DEFINITION

The received signal is composed of M components, each deterministic (except for unknown phase) and narrowband; also the signal components are essentially disjoint in time and/or frequency. The accompanying noise is zero-mean stationary Gaussian.

The receiver processor to be considered is depicted in Fig. 1. Input process

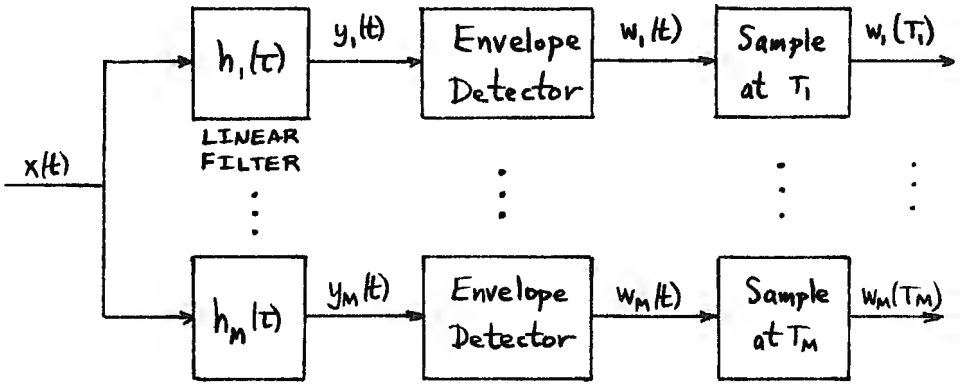

Fig. 1. Receiver Processor

x(t) is observed over time interval (a,b) and passed through a parallel set of M filters, each fairly well matched in time duration and frequency location to one of the M components of the received signal. The filter outputs are envelope-detected and sampled at different time instants, yielding a set of outputs $\{w_j(T_j)\}_1^M$. The method of combining these outputs for decisions on signal presence will be discussed shortly. Notice that the filters $\{h_j(\tau)\}_1^M$ are not required to be matched filters, but rather only have an impulse response duration approximately the same as the corresponding signal component, and have a frequency location approximately covering the signal components' spectral range. This allows a wide variety of sub-optimal receiver realizations to be considered and compared. Losses in performance due to mismatched receiving filters or improper gain settings of the filters are easily evaluated.

If just one signal component (M=1) were received, and phase-coherent reception were employed, instead of the phase-incoherent reception technique of Fig. 1 (i.e., no envelope detectors), the false alarm and detection probabilities are derived in Appendix A for an arbitrary filter and sampling instant, and then specialized to various optimum filter choices for different observation intervals and noise spectra. On the other hand, for phase-incoherent reception of one signal component, the false alarm and detection probabilities are derived in Appendix B, under conditions similar to Appendix A. These results are given for the sake of completeness and to indicate the method of performance comparison to be adopted for the M-component signal case.

For the M-component signal case, the optimum method of combining outputs $\{w_j(T_j)\}$ in Fig. 1 (even for non-optimum, but given, forms of filters $\{h_j(\tau)\}$) is derived in Appendix C. The difficulty of implementing and analyzing this processor suggests the simpler sub-optimum processor which combines the outputs according to

$$z = \sum_{j=1}^{M} w_j^2(T_j), \tag{1}$$

and compares z with a threshold. The characteristic function of decision variable z is derived in Appendix C, and the false alarm and detection probabilities given. Specialization of the general filter characteristics to optimum choices is also presented in Appendix C.

If it were possible to process the received waveform x(t) in Fig. 1 by a phase-coherent technique (which would require knowledge of the phase of each signal component), the performance, in terms of false alarm and detection probabilities, would be significantly improved for large M. It is the purpose of this memo to make this comparison quantitative, over a wide range of false alarm probabilities and number of components M. The false alarm and detection probabilities for coherent reception of the M-component signal are presented in Appendix D.

RESULTS

The characteristic function of decision variable z in (1) is given by (C17), and the false-alarm and detection probabilities are given by (C22) and (C19) respectively. The performance of the processor in Fig. 1 is characterized by the single parameter d_T, which is a measure of the total "output signal-to-noise (voltage) ratio." Specifically, from (C13), it is given by

$$d_T^2 = \sum_{j=1}^{M} \frac{\left| \int_a^b d\tau\, h_j(T_j - \tau)\, \underline{s}_j(\tau) \right|^2}{\frac{1}{2} \iint_a^b d\tau_1\, d\tau_2\, \underline{h}_j(T_j - \tau_1)\, \underline{h}_j^*(T_j - \tau_2) R_n(\tau_1 - \tau_2)}, \tag{2}$$

where $\underline{h}_j(\tau)$ is the complex envelope of filter $h_j(\tau)$, $\underline{s}_j(t)$ is the complex envelope of the j-th component of the received signal, and $R_n(\tau)$ is the correlation function of the complex envelope of the received noise. The filters in (2) are not assumed to be matched filters, but are general, subject only to

the constraint that their impulse response durations and bandwidths be approximately the same as the corresponding signals. The detailed assumptions and derivations leading to (2) are documented in Appendix C.

Plots of detection probability P_D (in per cent) versus d_T, for false alarm probability P_F equal to 10^{-2}, 10^{-4}, 10^{-6}, and 10^{-8}, are presented in Figs. 2-17, for M=1(1) 10, 16, 32, 64, 128, 256, 512*, respectively. (There is a change of abscissa scale for $M \geq 32$). As M increases, the performance for a given value of d_T degrades. For example, to attain $P_F = 10^{-8}$, $P_D = .5$, a value for d_T of 6 is required for M=1, whereas a value for d_T of 16.6 is required for M=512; this is an increase of $20 \log(16.6/6) = 8.84$dB in signal-to-noise ratio. Thus fractionalization of a fixed amount of signal energy degrades the processor performance.

This behavior is made more obvious by constructing the cross-plots in Figs. 18-21 of detection probability P_D versus d_T, with false alarm probability P_F held fixed, for M = 1(1) 6, 8, 10. (The curves for larger values of M can be found, if desired, from Figs. 12-17).

Figures 2-21 constitute the receiver operating characteristics (ROC) for the processor depicted in Fig. 1 followed by squaring and summation. We now wish to compare this performance with that of a processor capable of coherently summing up all M signal components. (We do not necessarily require the coherent processor to be optimum; this aspect of the problem is considered in Appendix D, where connections with the optimum filters for the phase-incoherent processor are made). The false alarm and detection probabilities of the coherent processor are given in (A13), where the parameter d_c is given by (A12).

The method of comparison of the processors is as follows: both processors are required to yield the same P_F, P_D. The required numerical value of d_c for the coherent processor is then smaller than the value of d_T required for the phase-incoherent processor of Fig. 1. The increased amount of signal-to-noise ratio required by the incoherent processor is then given by

*The crosses on Fig. 17 will be explained in the next section.

$$20 \log (d_T/d_c), \text{ in dB,} \tag{3}$$

since both d_T and d_c are measures of signal-to-noise voltage ratios. (See also Appendices B and D for comparison of the optimum processors). In Figs. 22-24, (3) is plotted versus the number of signal components M, with false-alarm probability P_F as a parameter, for detection probability P_D equal to .5, .9, .99, respectively. (There is an ordinate scale change in Fig. 23. Also straight lines have been drawn between the integer abscissa values for ease of interpretation). It is seen that for a specified detection probability, the increase in required signal-to-noise ratio is greater for the lower false-alarm probabilities; for example, for $P_D = .5$, M=10, the increase in signal-to-noise ratio must be 5.33dB at $P_F = 10^{-2}$, but only 2.69 dB at $P_F = 10^{-8}$. It is also to be noted that the increase in required signal-to-noise ratio for the phase-incoherent processor is greater for the lower detection probabilities; for example, for $P_F = 10^{-2}$, M = 10, the numbers are 5.33dB at $P_D = .5$, 4.15dB at $P_D = .9$, and 3.55dB at $P_D = .99$. Thus the greatest discrepancy in performance between the coherent and incoherent processors occurs at the lower detection and false-alarm probabilities.

In Figs. 25-27, similar results extending up to M = 512 are plotted on logarithmic paper. The curves appear to be approaching a 5 logM dependence for large M. For large M, significantly larger signal-to-noise ratios are required; for example 13dB more is required at $P_D = .5$, $P_F = 10^{-2}$, M = 512 for the incoherent versus coherent processor. (Recall that the ordinates of Figs. 22-27 are the increased signal-to-noise ratios, and not the actual values of signal-to-noise ratio required for a specified performance).

GAUSSIAN APPROXIMATION

In Appendix E, the decision variable z in (1) is approximated by a Gaussian random variable with the same mean and variance. The detection and false-alarm probabilities are given by (E12). For large M, this is expected to be a good approximation, since (1) is the sum of a large number of independent random variables. For M = 512, the Gaussian approximation is plotted as crosses on Fig. 17; it is seen to be a very good one for $P_F = 10^{-2}$, but slightly poorer at $P_F = 10^{-2}$. Thus the Gaussian approximation can be used for other values of M with a known degree of accuracy established from Fig. 17.

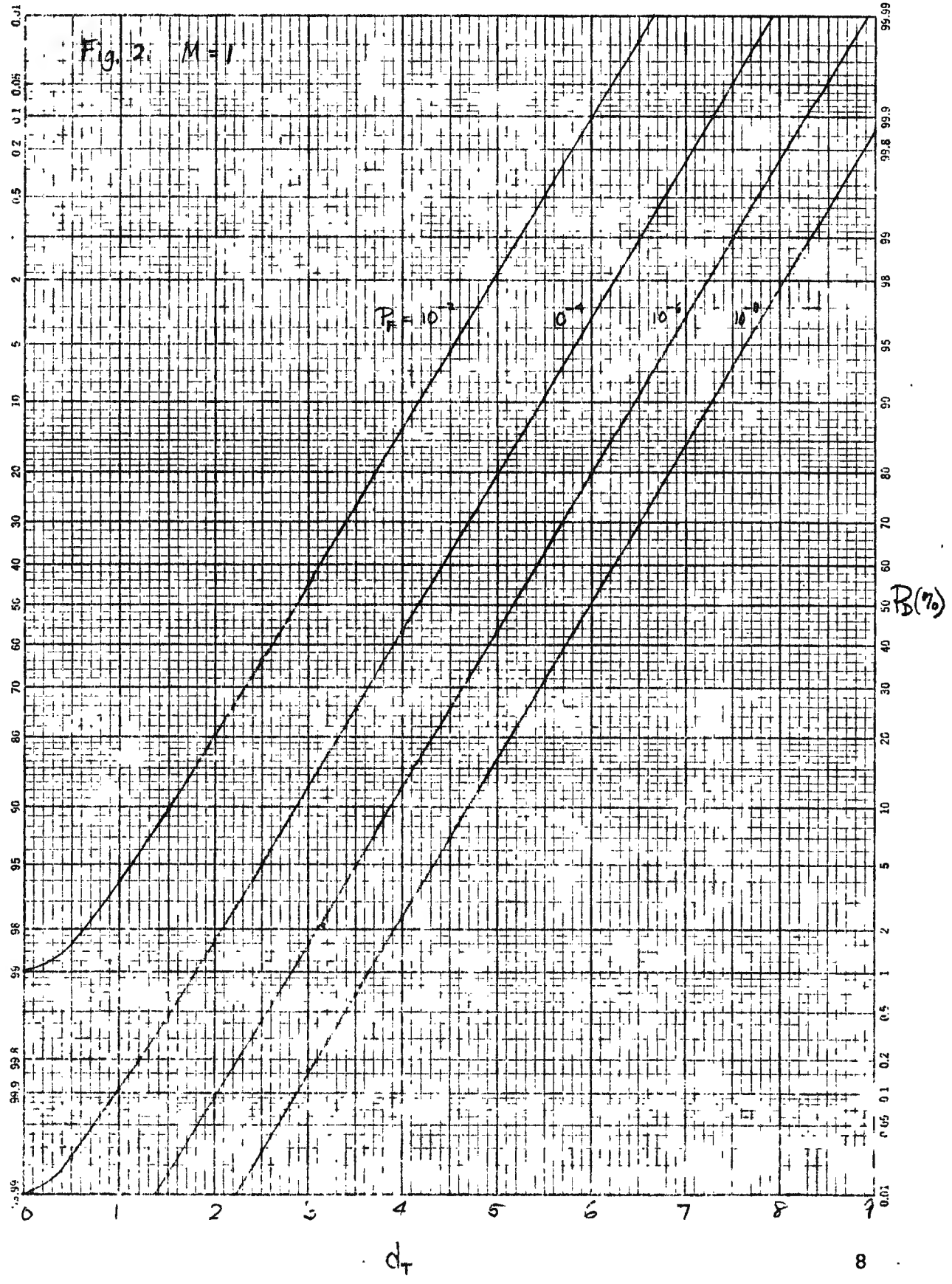
Fig. 2 M=1
$P_F = 10^{-3}$
10^{-4}
10^{-5}
10^{-6}
$P_B(\%)$
d_T

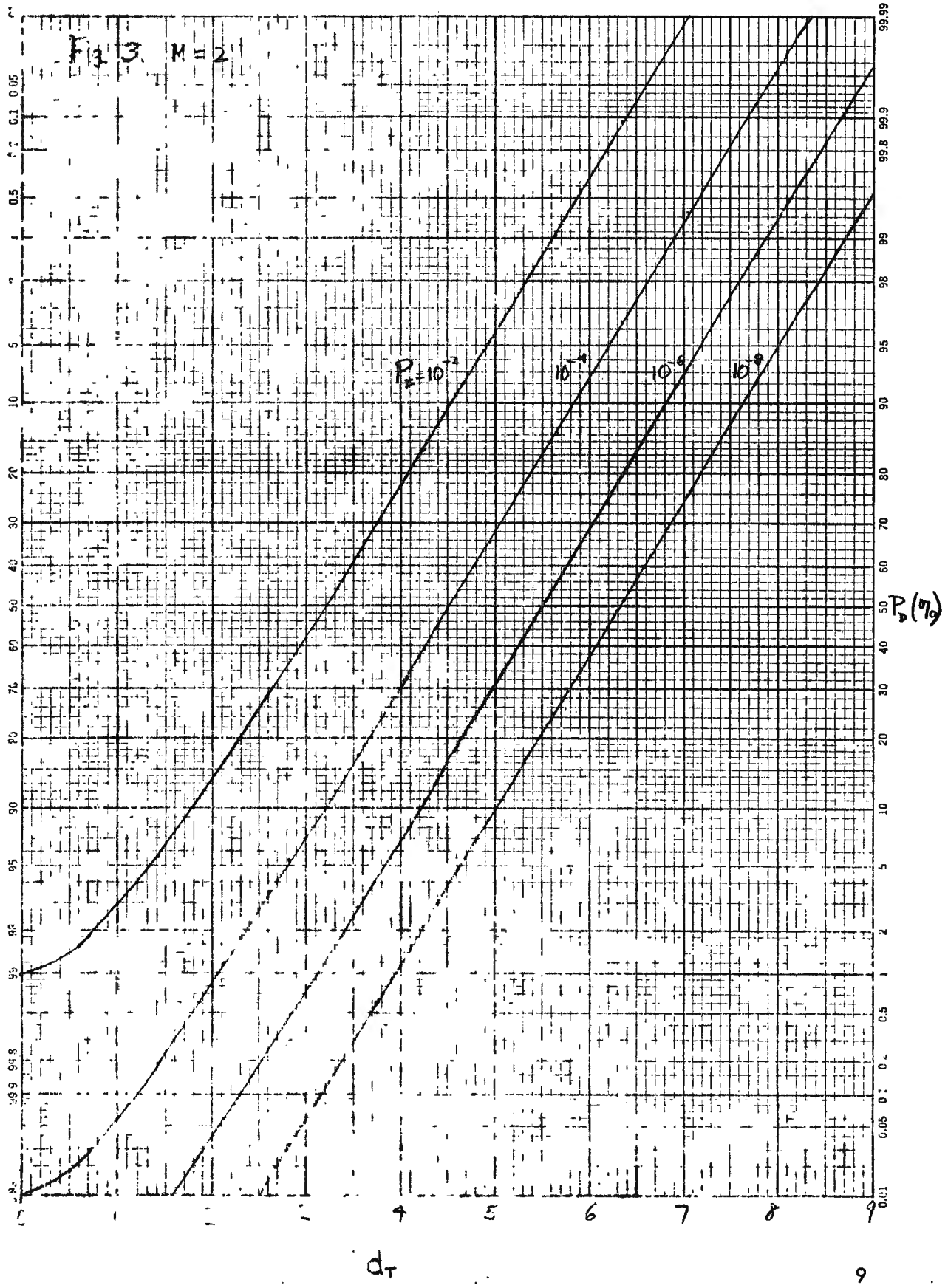
Fig 3. M = 2
$P_e = 10^{-2}$
10^{-4}
10^{-6}
10^{-8}
P_b (%)
d_T

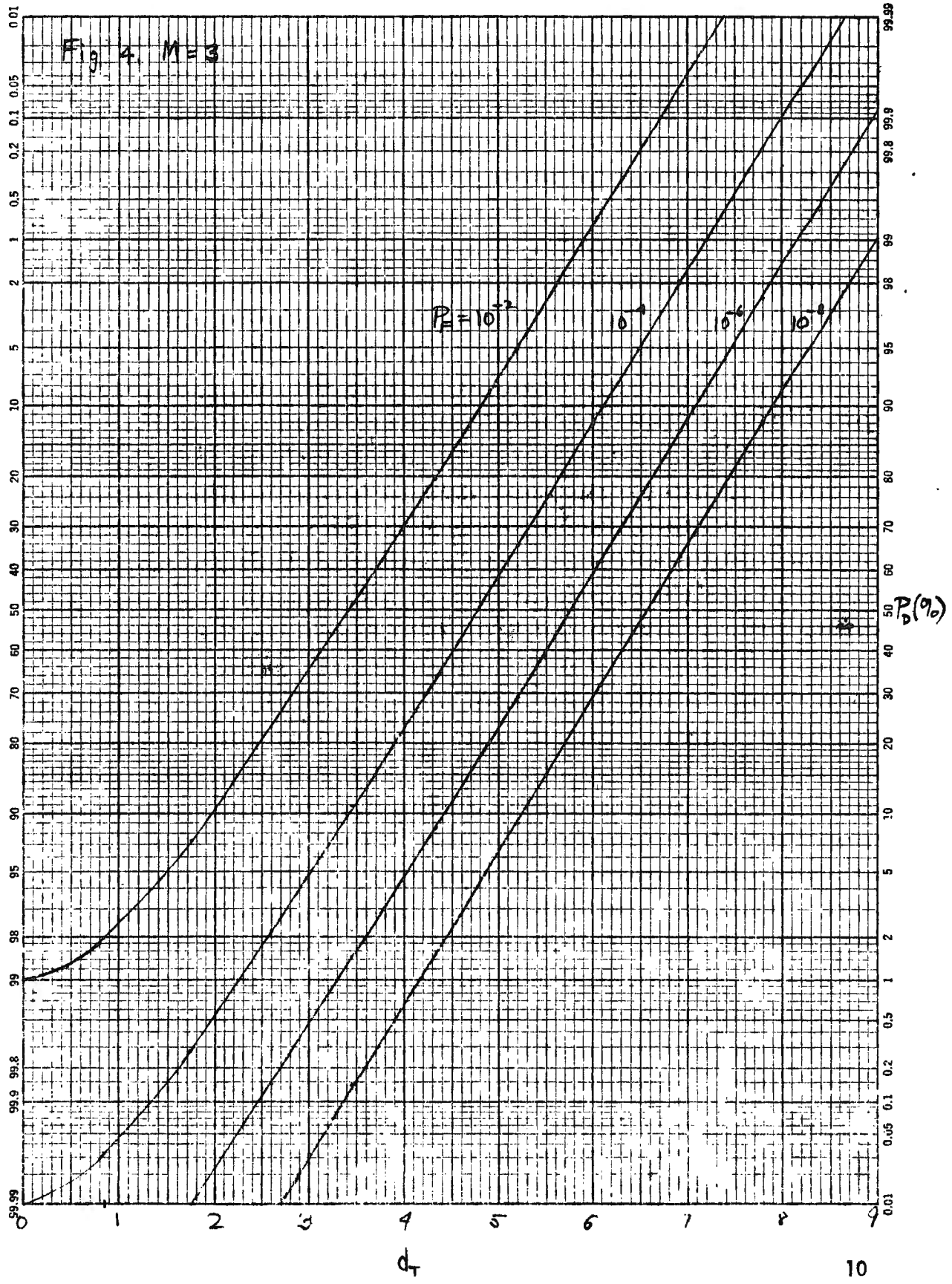
Fig 4. M=3
$P_F = 10^{-2}$
10^{-4}
10^{-6}
10^{-8}
$P_D(\%)$
d_T
0
1
2
3
4
5
6
7
8
9

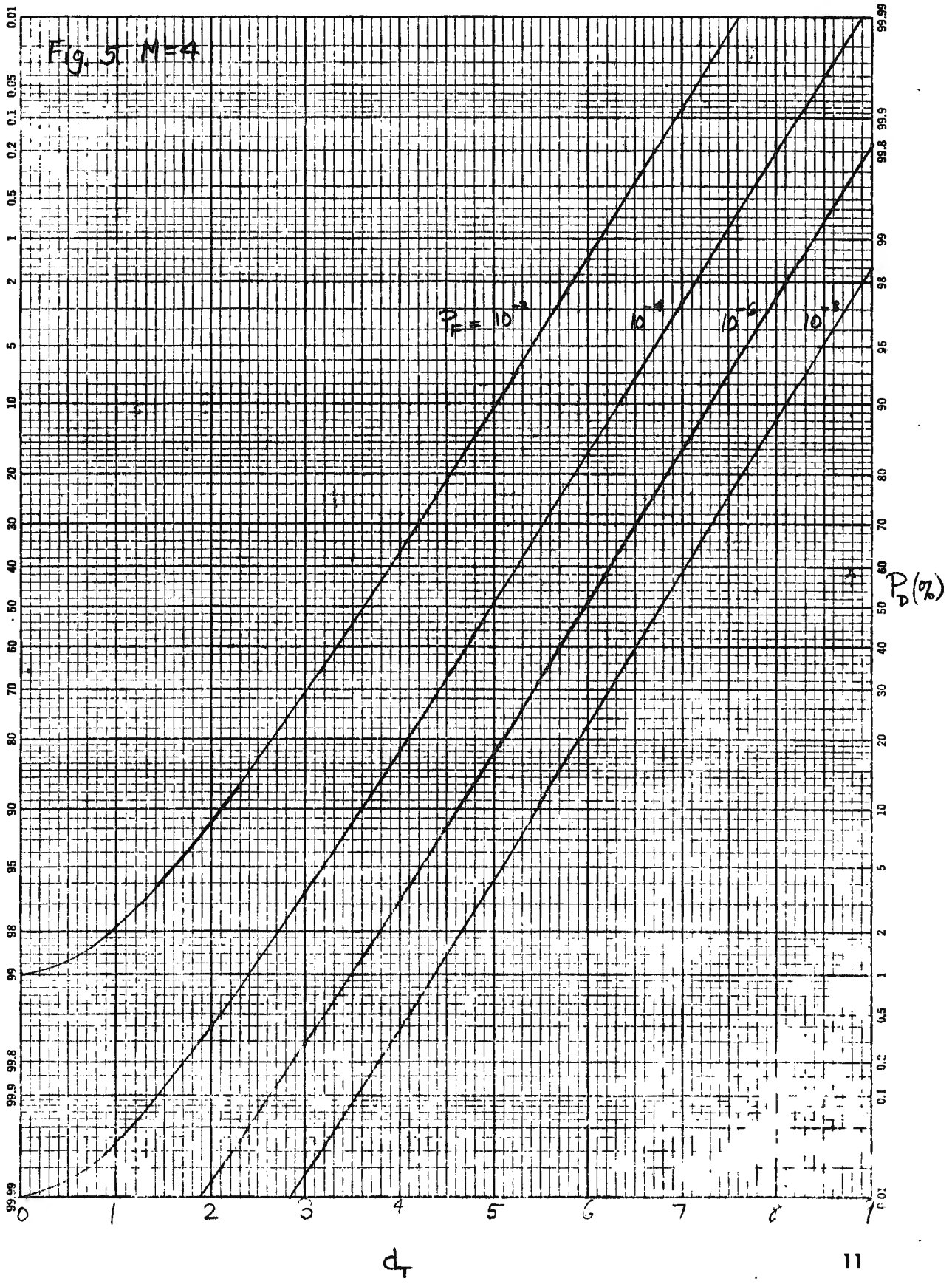
Fig. 5 M=4
$P_F = 10^{-2}$
10^{-4}
10^{-6}
10^{-8}
P_D(%)
0.01
0.05
0.1
0.2
0.5
1
2
5
10
20
30
40
50
60
70
80
90
95
98
99
99.8
99.9
99.99
0
1
2
3
4
5
6
7
8
d_T

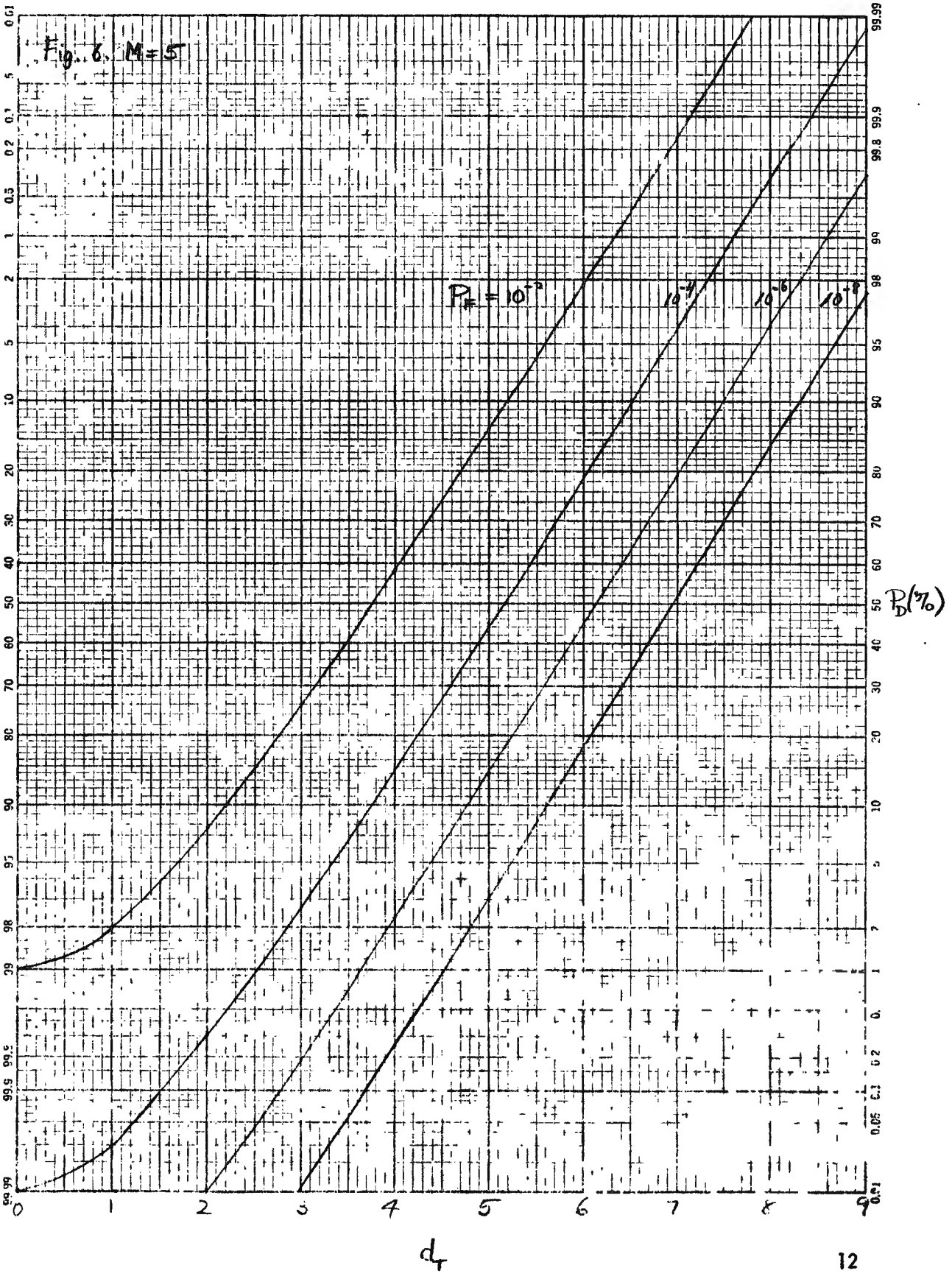
Fig. 6. M=5
$P_F = 10^{-2}$
10^{-4}
10^{-6}
10^{-8}
P_D(%)
d_T

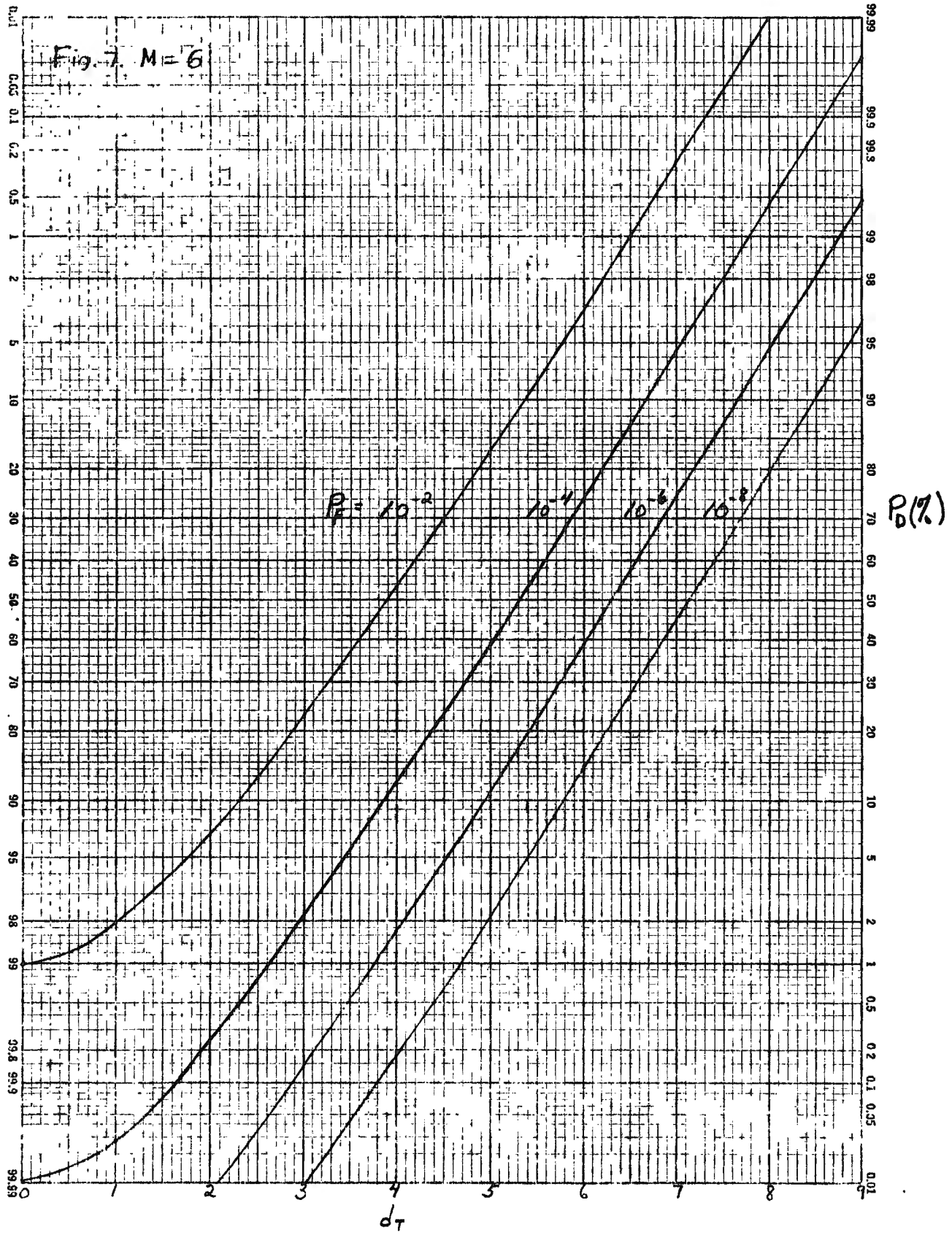
Fig. 7. M=6
$P_F = 10^{-2}$
10^{-4}
10^{-6}
10^{-8}
$P_D(\%)$
d_T
0
1
2
3
4
5
6
7
8
9
99.99
99.9
99.8
99
98
95
90
80
70
60
50
40
30
20
10
5
2
1
0.5
0.2
0.1
0.05
0.01
0.1
0.05
0.2
0.5
1
2
5
10
20
30
40
50
60
70
80
90
95
98
99
99.8
99.9
99.99

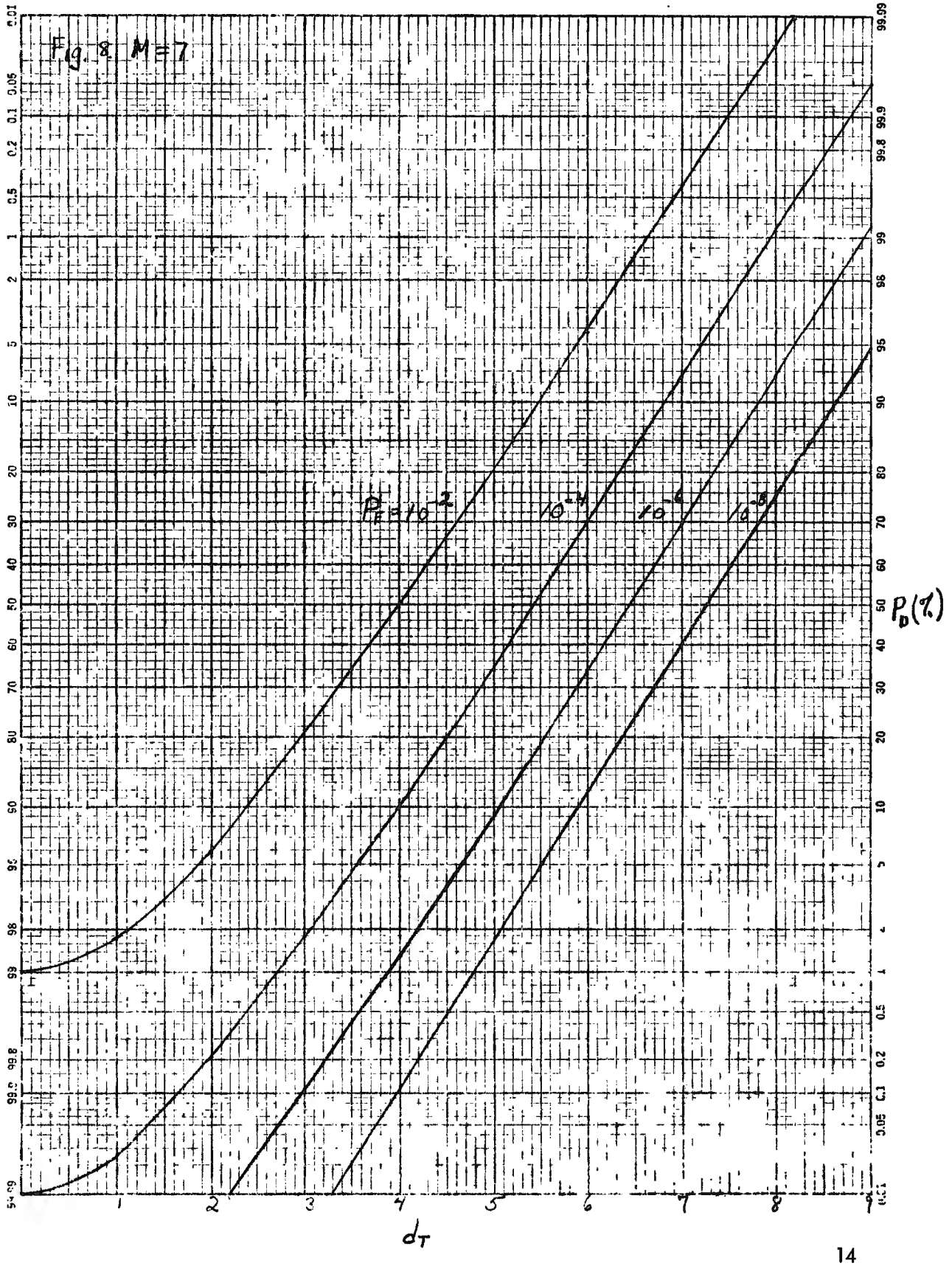
Fig. 8 M=7
$P_F = 10^{-2}$
10^{-4}
10^{-6}
10^{-8}
$P_D(\%)$
d_T

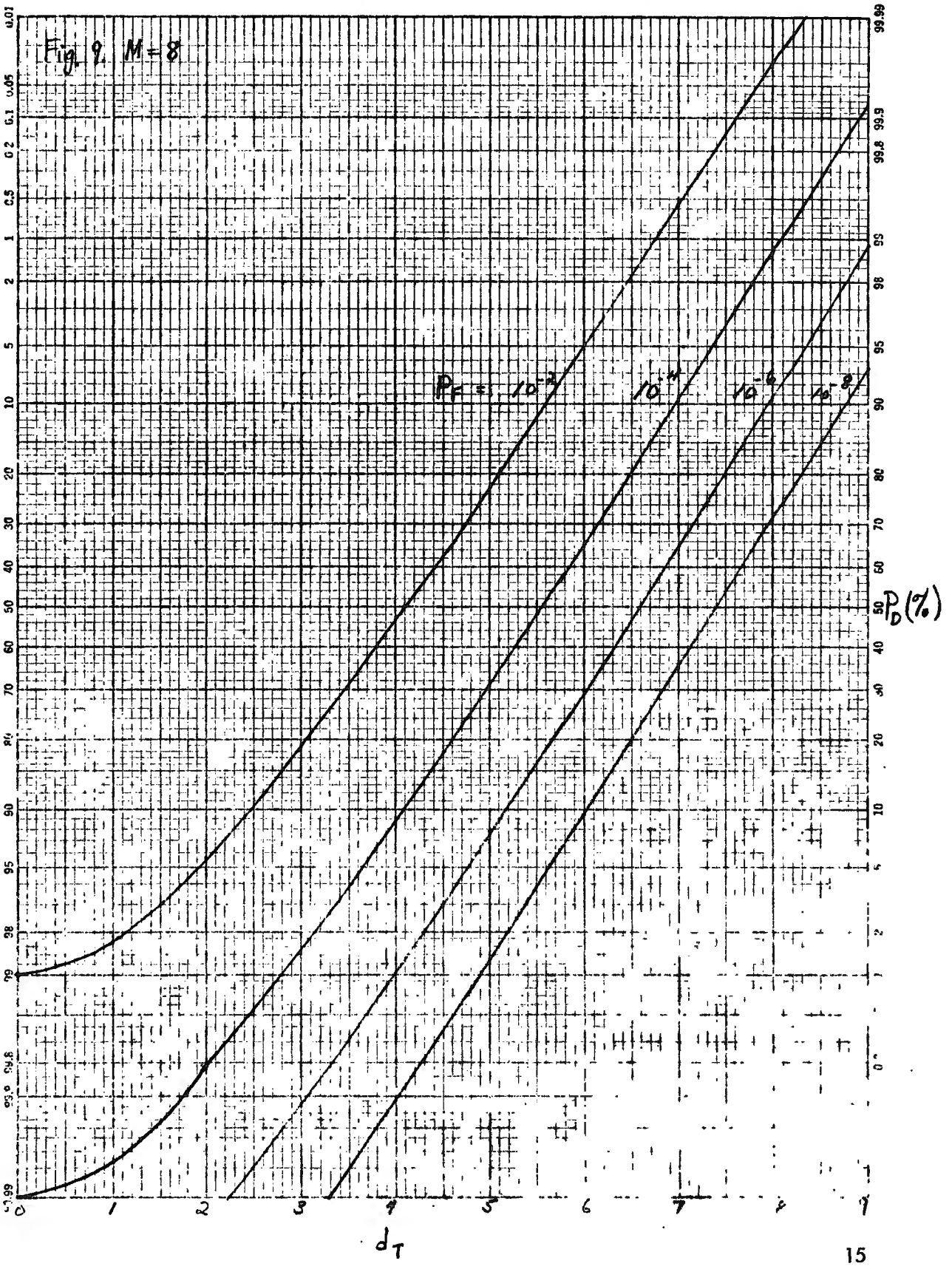
Fig. 9. M=8
$P_F = 10^{-2}$
10^{-4}
10^{-6}
10^{-8}
P_D (%)
d_T

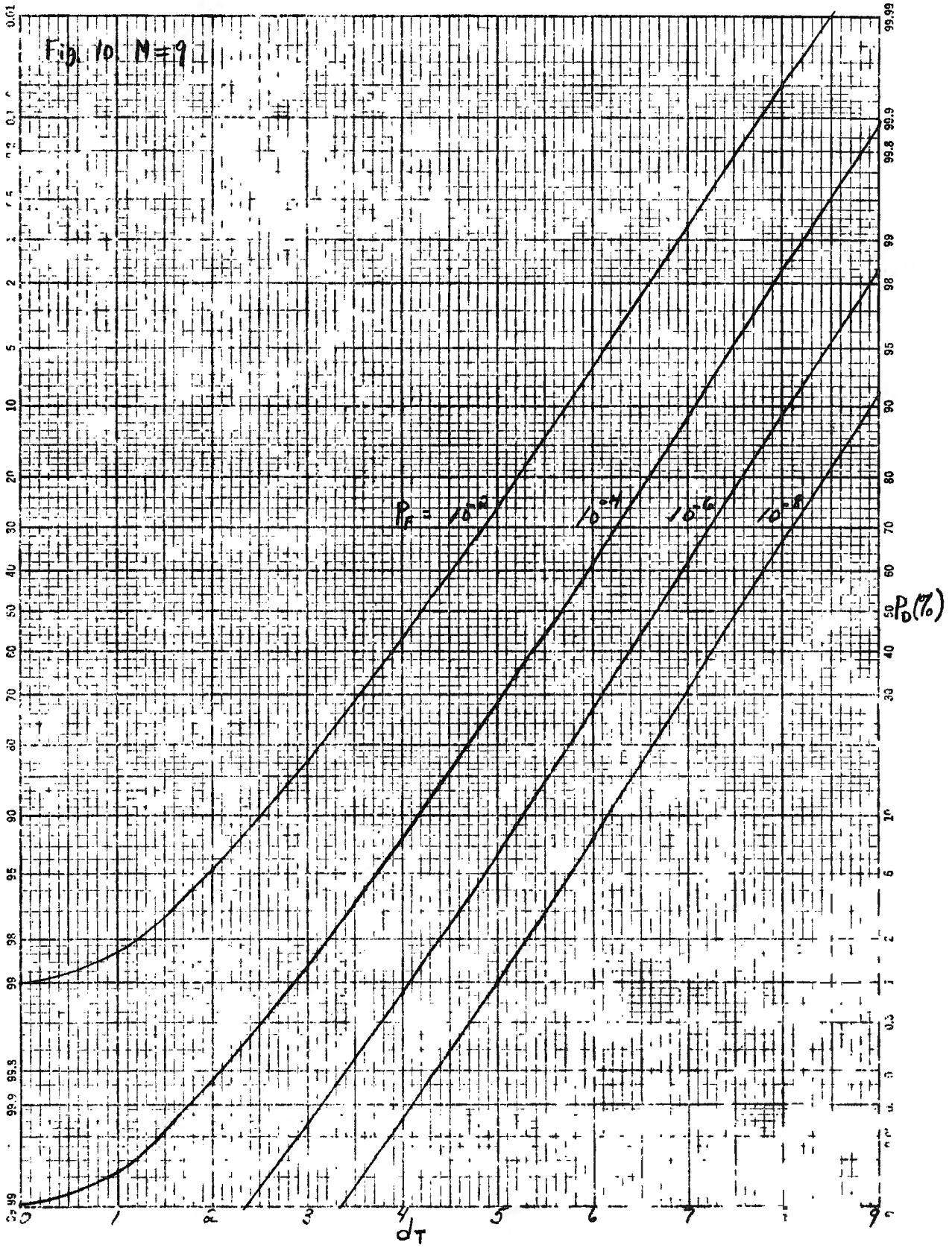
Fig. 10 N=9
$P_E = 10^{-2}$
10^{-4}
10^{-6}
10^{-8}
P_D(%)
d_T

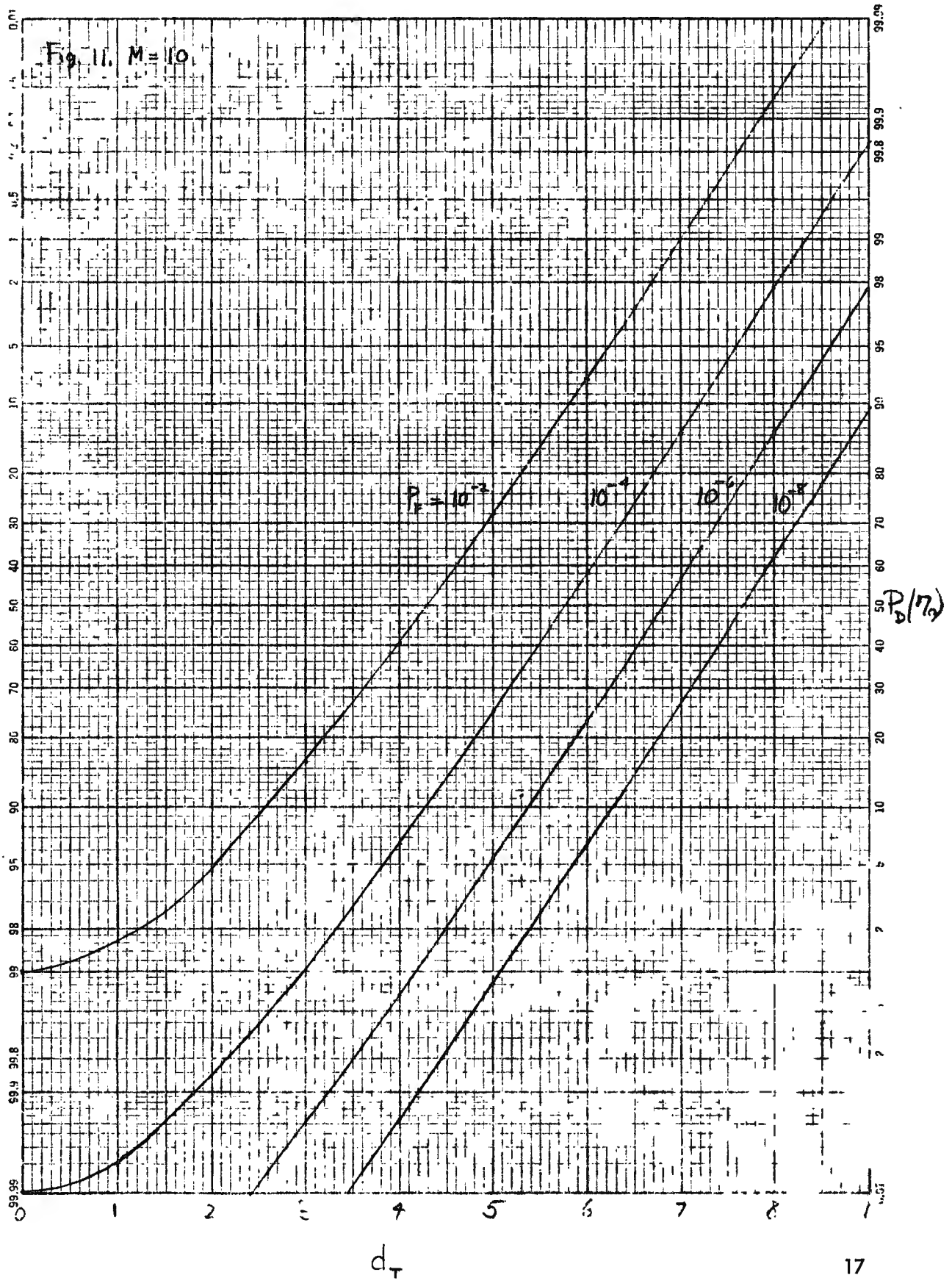
Fig. 11. M = 10
$P_F = 10^{-2}$
10^{-4}
10^{-6}
10^{-8}
$P_D(/n)$
d_T

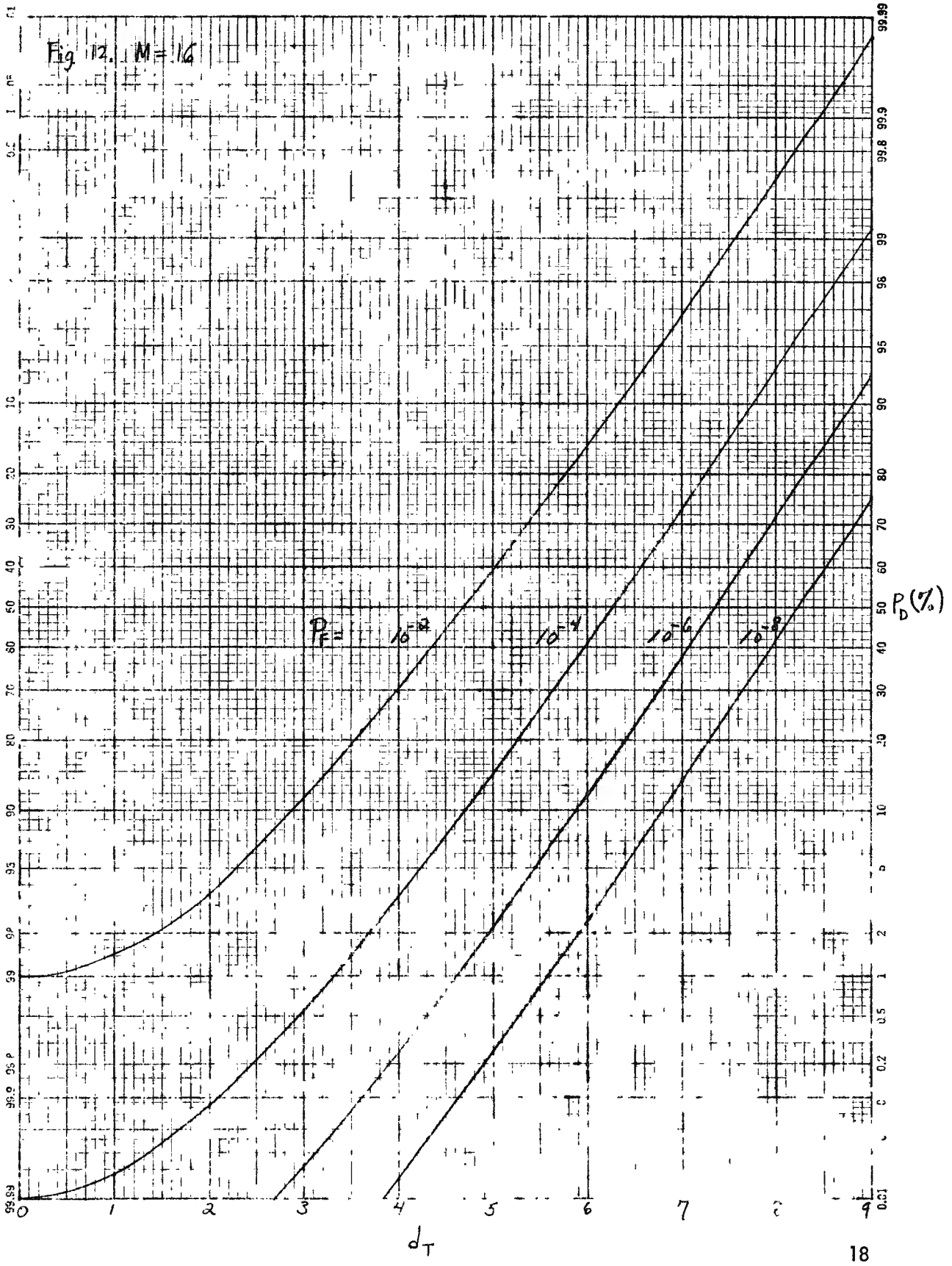
Fig 12. M = 16
$P_F =$ 10^{-2}
10^{-4}
10^{-6}
10^{-8}
P_D (%)
99.99
99.9
99.8
99
98
95
90
80
70
60
50
40
30
20
10
5
2
1
0.5
0.2
0.1
0.01
0
1
2
3
4
5
6
7
8
9
d_T

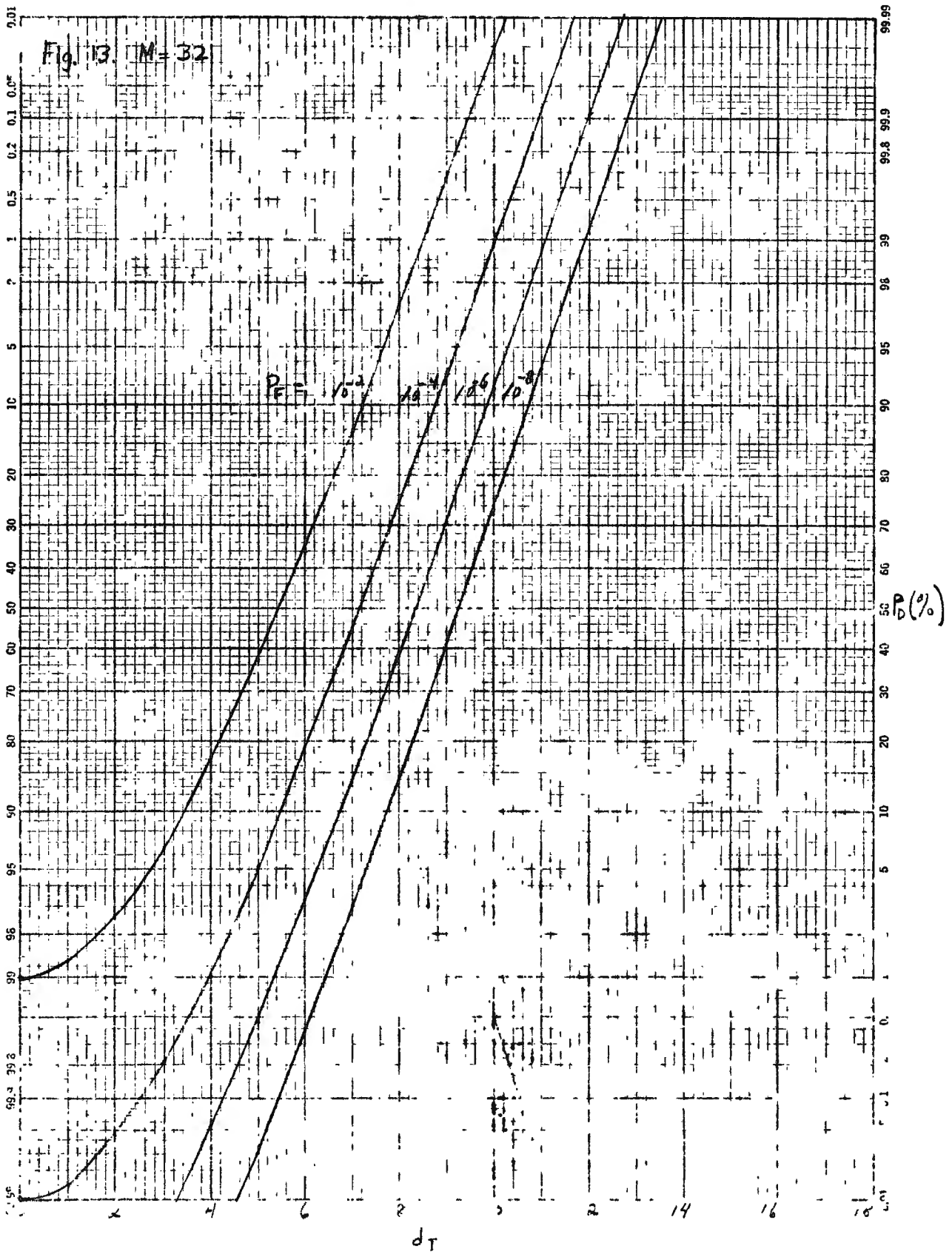
Fig. 13. M=32
$P_F =$ 10^{-2} 10^{-4} 10^{-6} 10^{-8}
P_D (%)
d_T

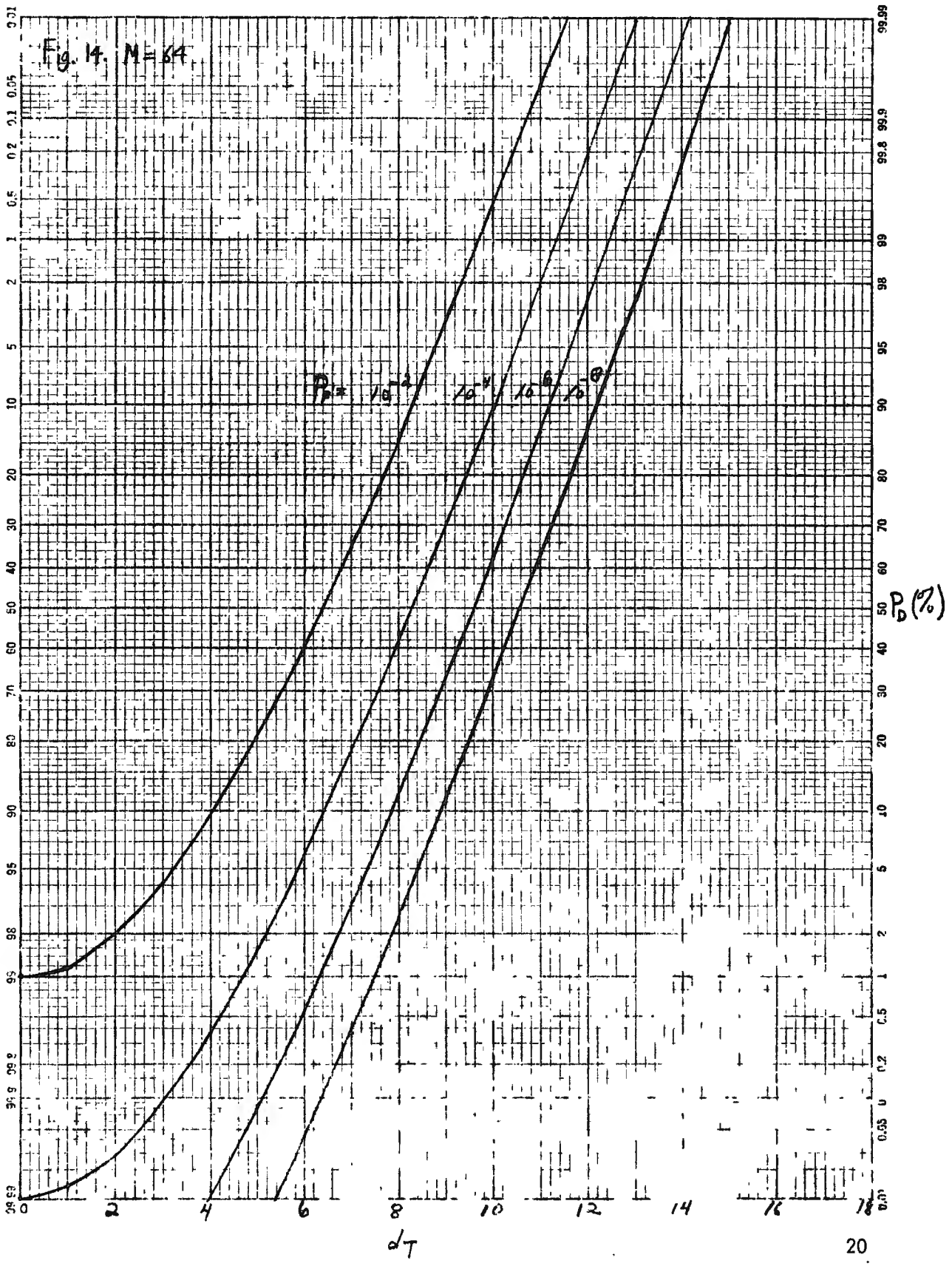
Fig. 14. M=64
P_b= 10^{-2} 10^{-4} 10^{-6} 10^{-8}
P_D (%)
d_T
0
2
4
6
8
10
12
14
16
18

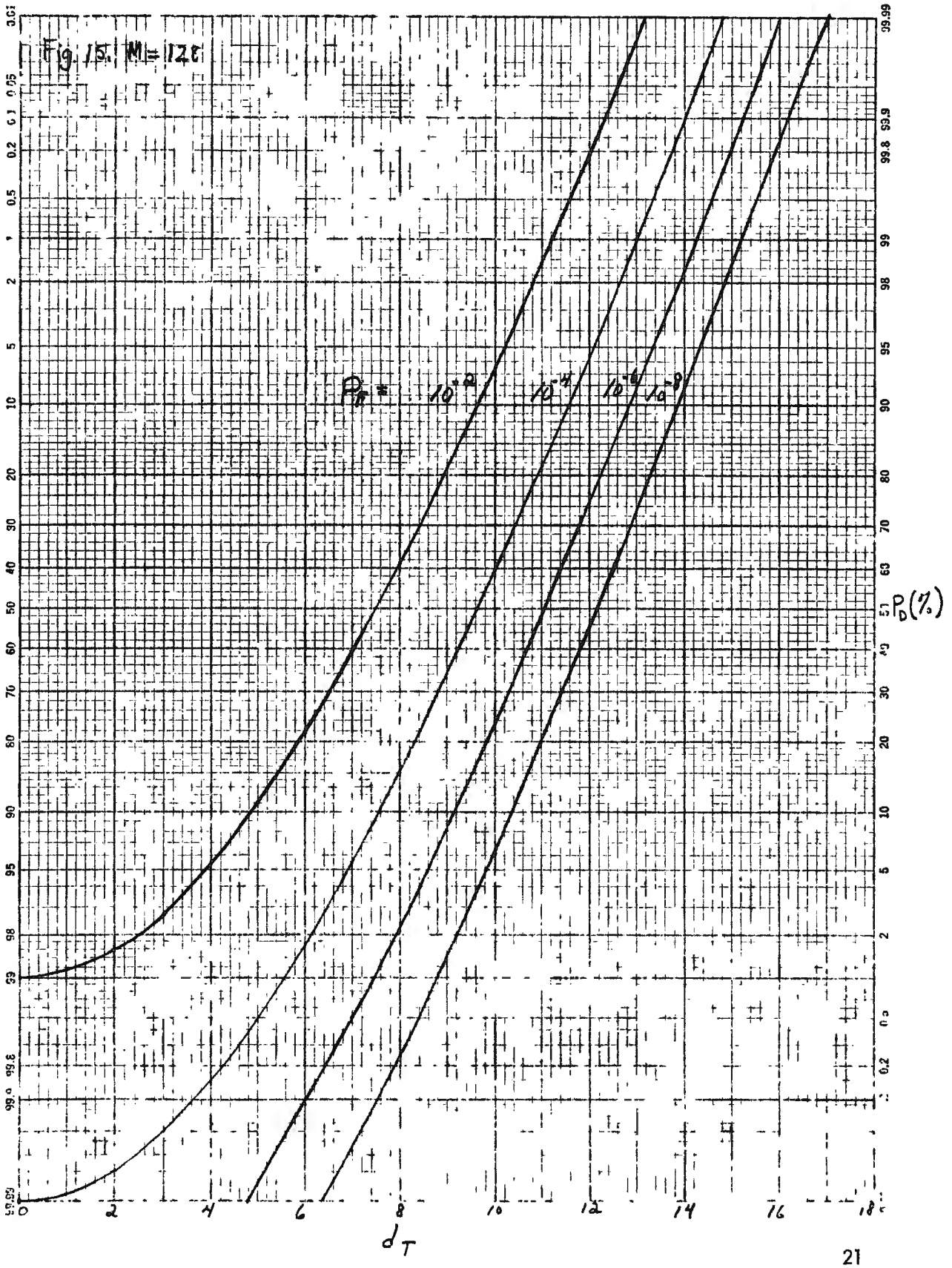
Fig 15. M=128
P_{fa} = 10^{-2} 10^{-4} 10^{-6} 10^{-8}
P_D(%)
d_T

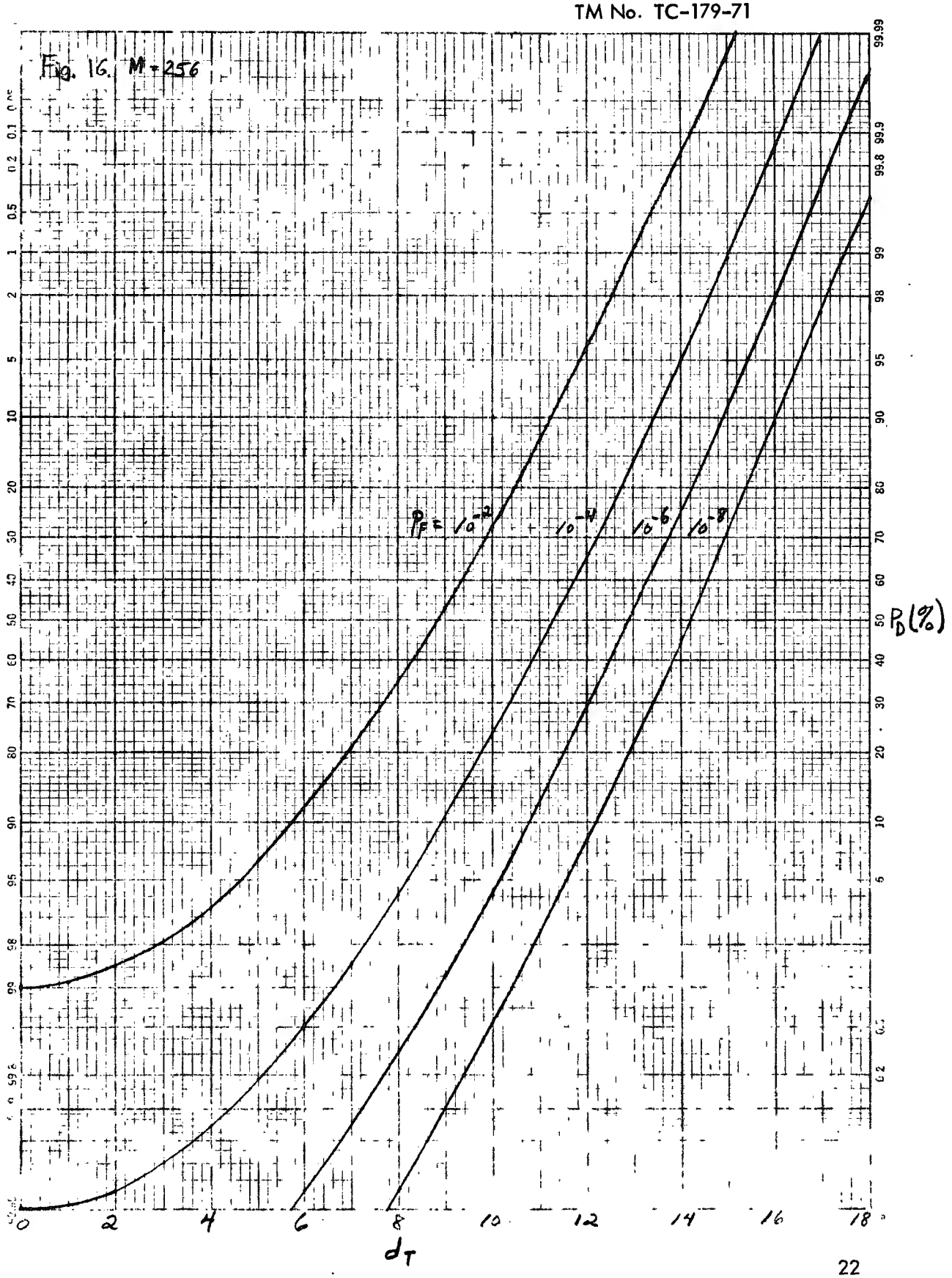
Fig. 16. M=256
$P_F = 10^{-2}$
10^{-4}
10^{-6}
10^{-8}
P_D (%)
99.99
99.9
99.8
99
98
95
90
80
70
60
50
40
30
20
10
6
0.2
0.1
0.5
1
2
5
0
2
4
6
8
10
12
14
16
18
d_T

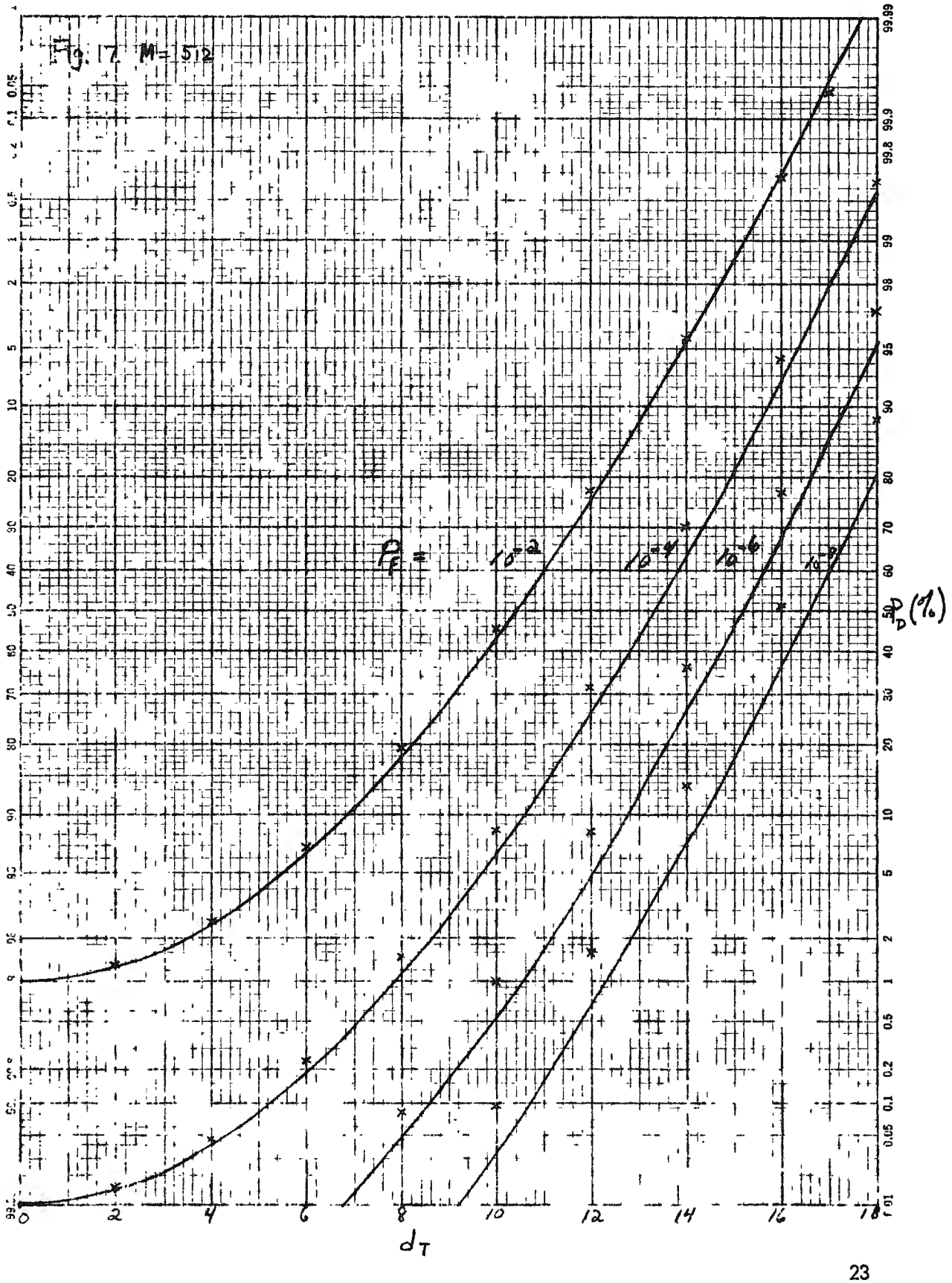
Fig. 17 M = 512
P_E =
10^{-2}
10^{-4}
10^{-6}
10^{-8}
$\frac{50}{D}$ (%)
d_T
0
2
4
6
8
10
12
14
16
99.99
99.9
99.8
99
98
95
90
80
70
60
50
40
30
20
10
5
2
1
0.5
0.2
0.1
0.05
0.01

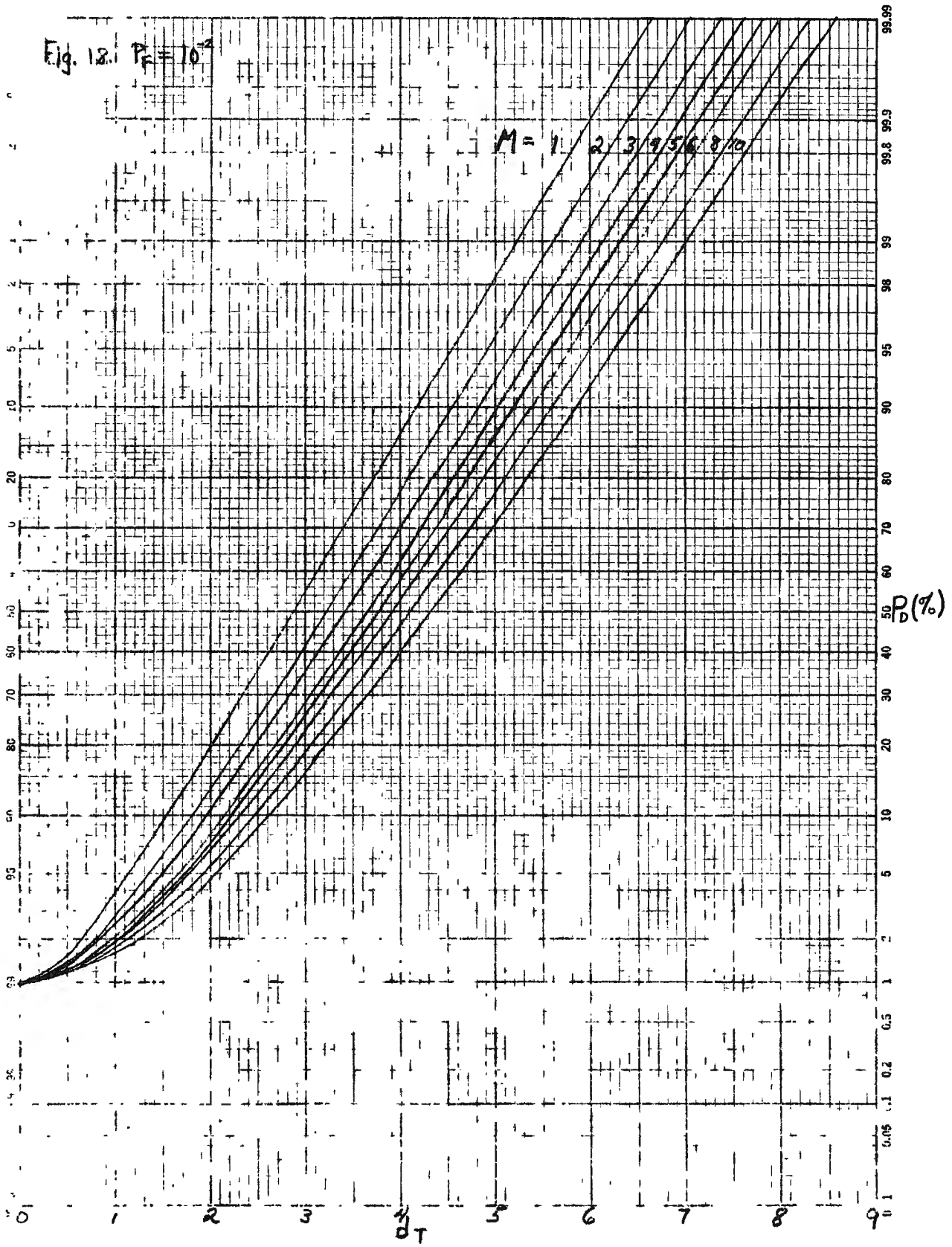
Fig. 12. $P_F = 10^{-2}$
M = 1 2 3 4 5 6 8 10
P_D(%)
$\frac{1}{D_T}$

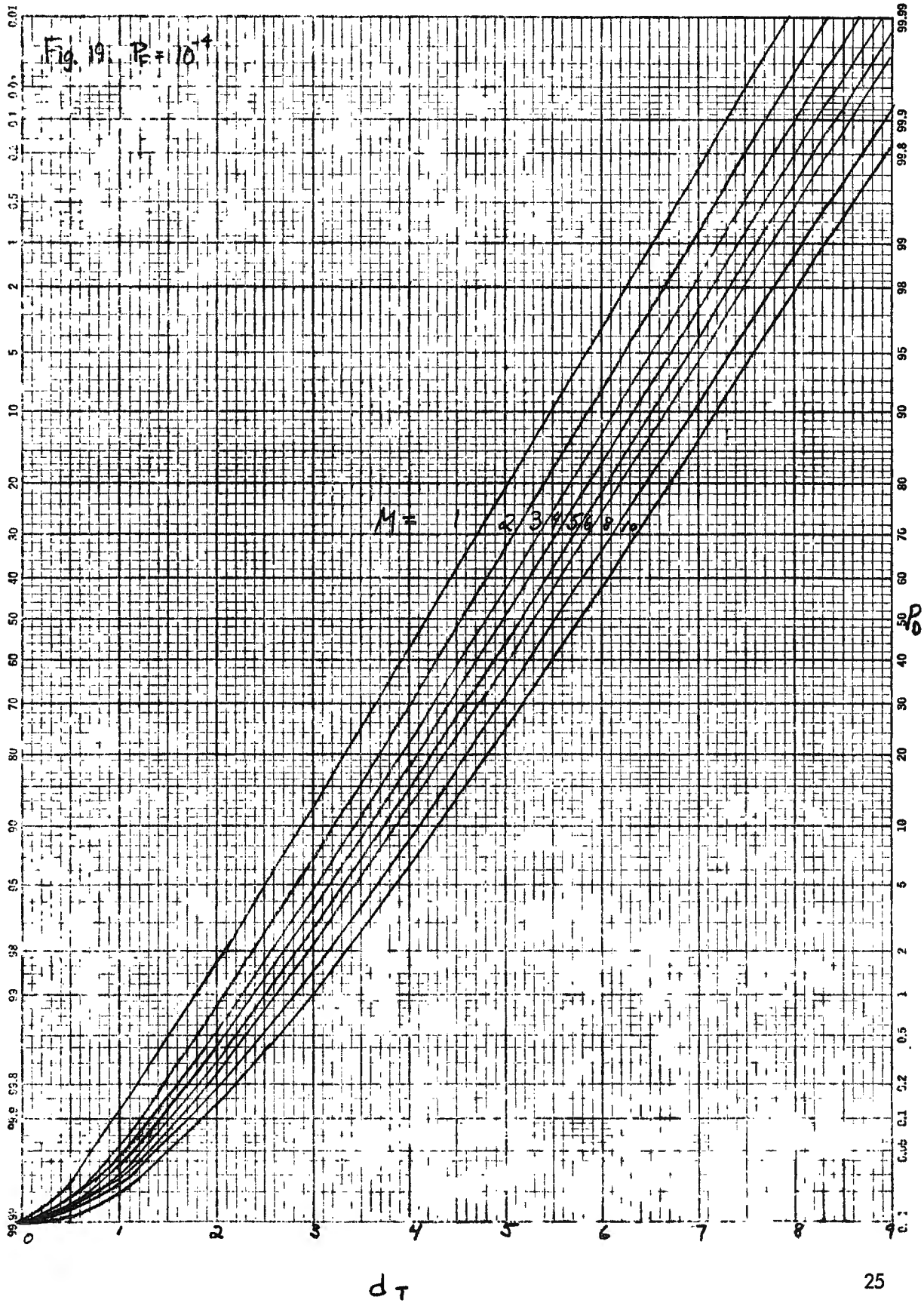
Fig. 19. $P_F = 10^{-4}$
M = 1 2 3 4 5 6 8 10
P_D(%)
d_T

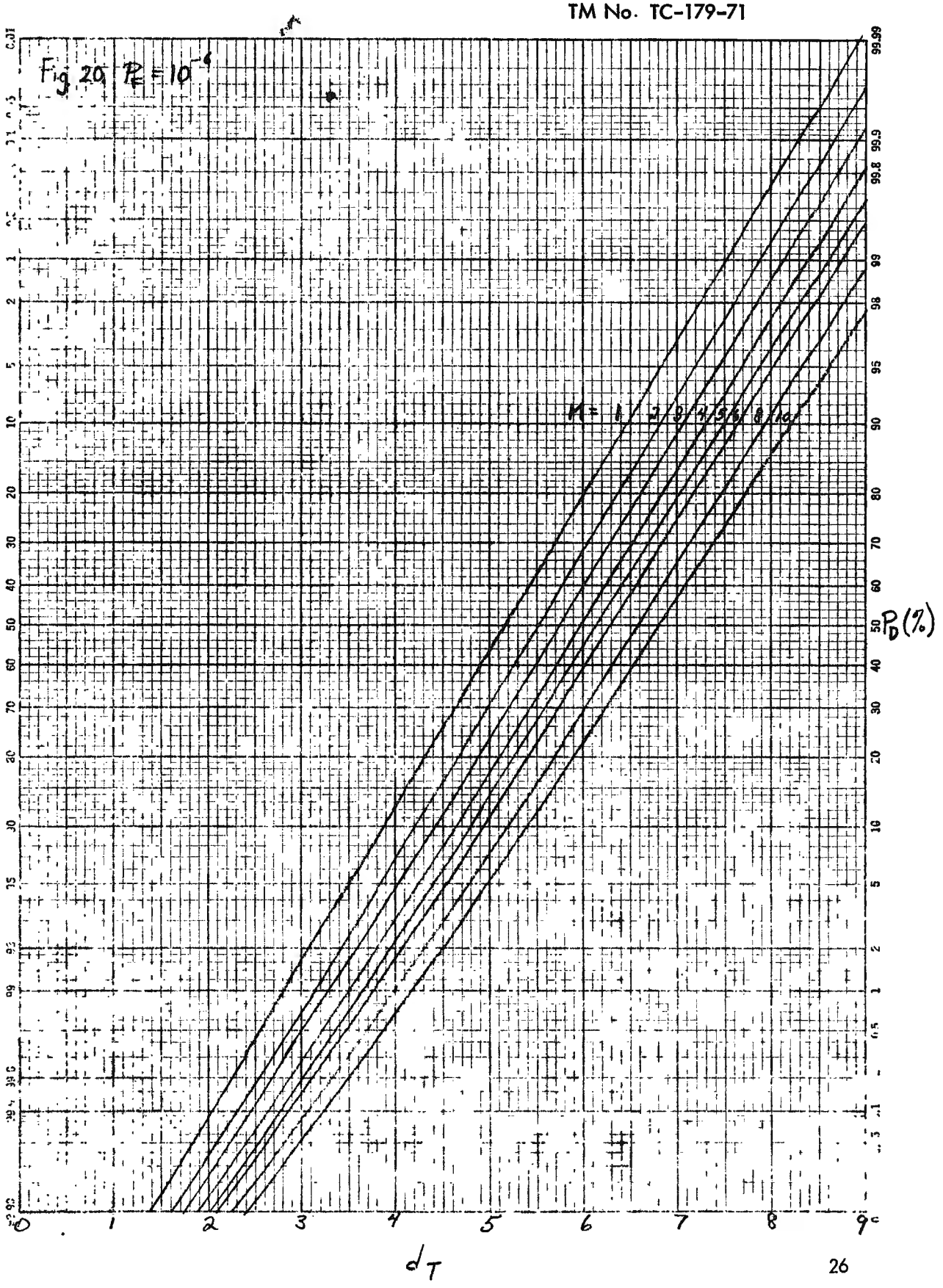
Fig 20 $P_E = 10^{-4}$
M = 1 / 2 / 3 / 4 / 5 / 6 / 8 / 10
P_D (%)
d_T
0 1 2 3 4 5 6 7 8 9
99.99 99.9 99.8 99 98 95 90 80 70 60 50 40 30 20 10 5 2 1

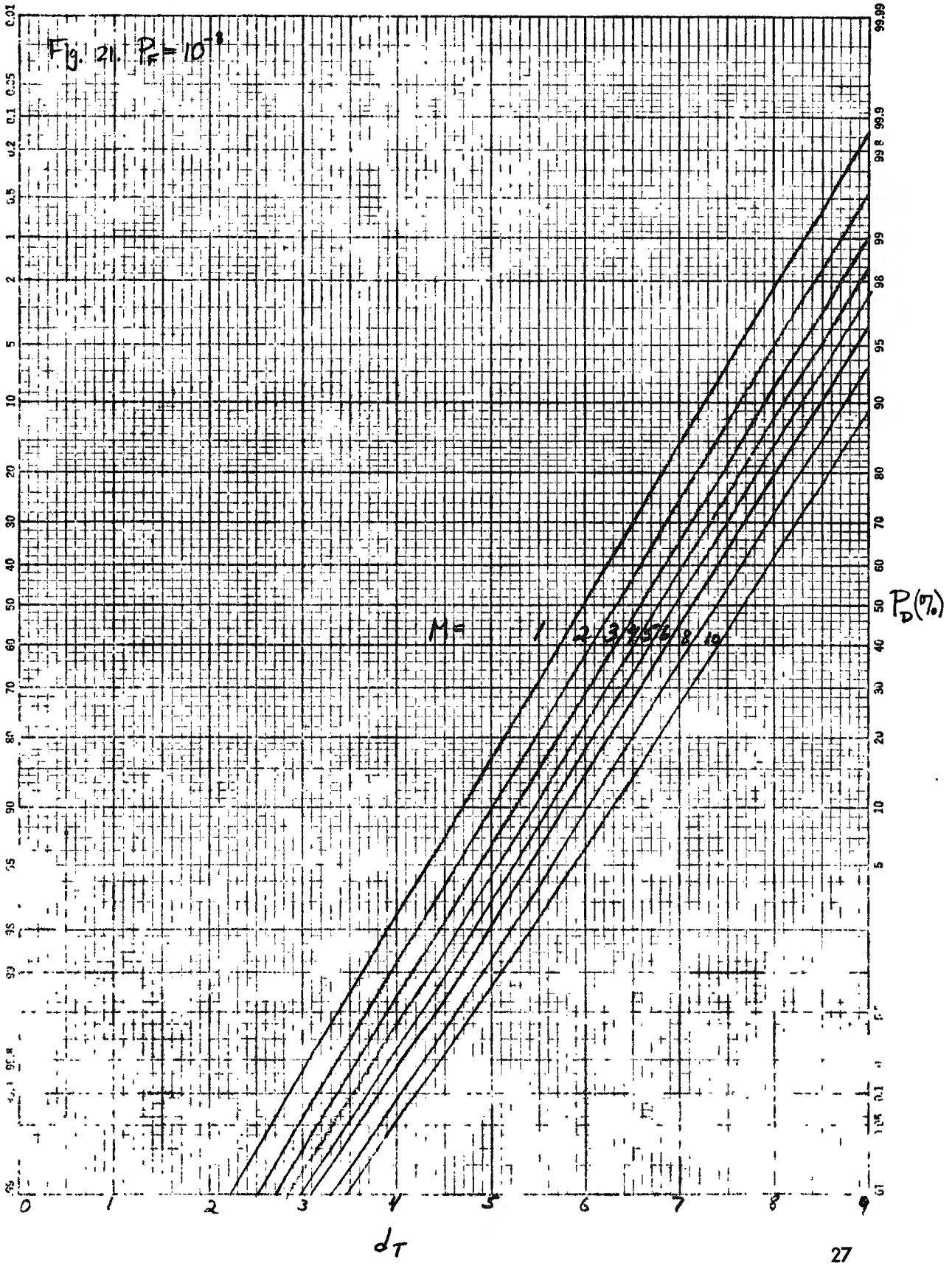
Fig. 21. $P_F = 10^{-9}$
M = 1 2 3 4 5 6 7 8 10
P_D (%)
d_T
0 1 2 3 4 5 6 7 8 9
99.99 99.9 99 98 95 90 80 70 60 50 40 30 20 10 5 2 1 0.5 0.2 0.1 0.05 0.01

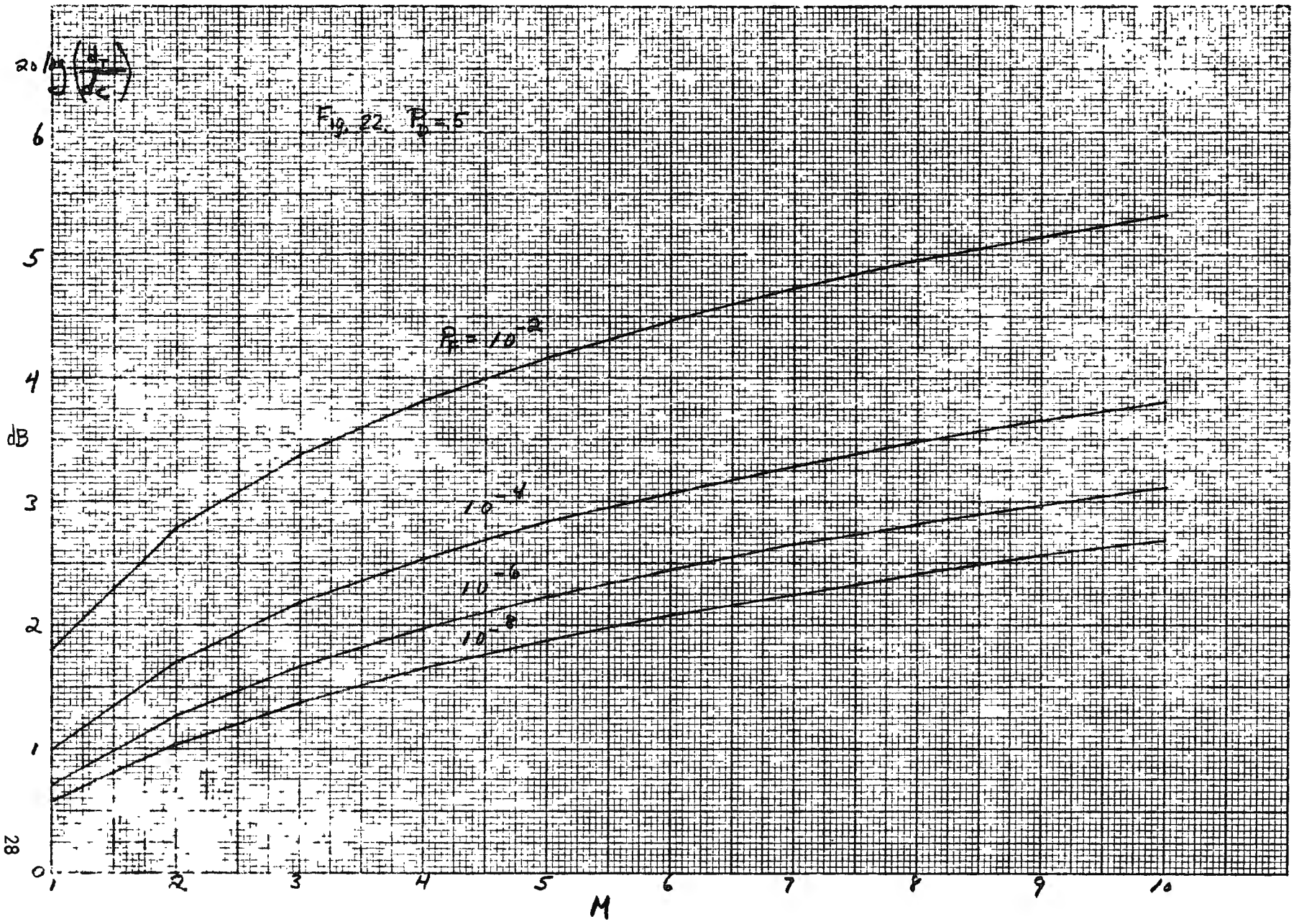
$20 \log \left(\frac{q_T}{q_c} \right)$
$F_{ig.}$ 22 $P_D = .5$
$P_{FA} = 10^{-2}$
10^{-4}
10^{-6}
10^{-8}
dB
M
0
1
2
3
4
5
6
7
8
9
10

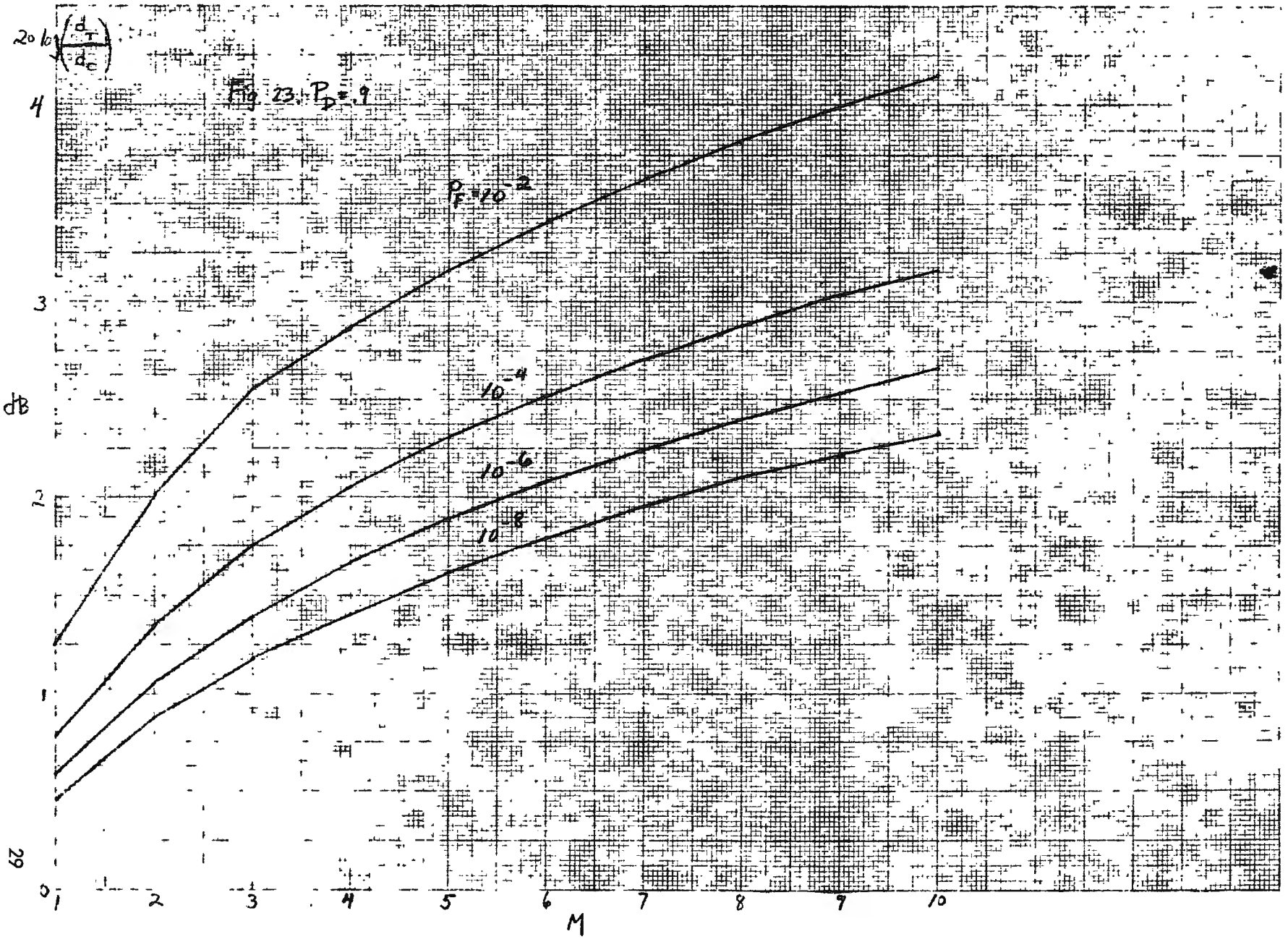
20 log (d_T / d_c)
Fig 23. P_D = .9
P_F = 10^-2
10^-4
10^-6
10^-8
dB
M
0
1
2
3
4
1
2
3
4
5
6
7
8
9
10

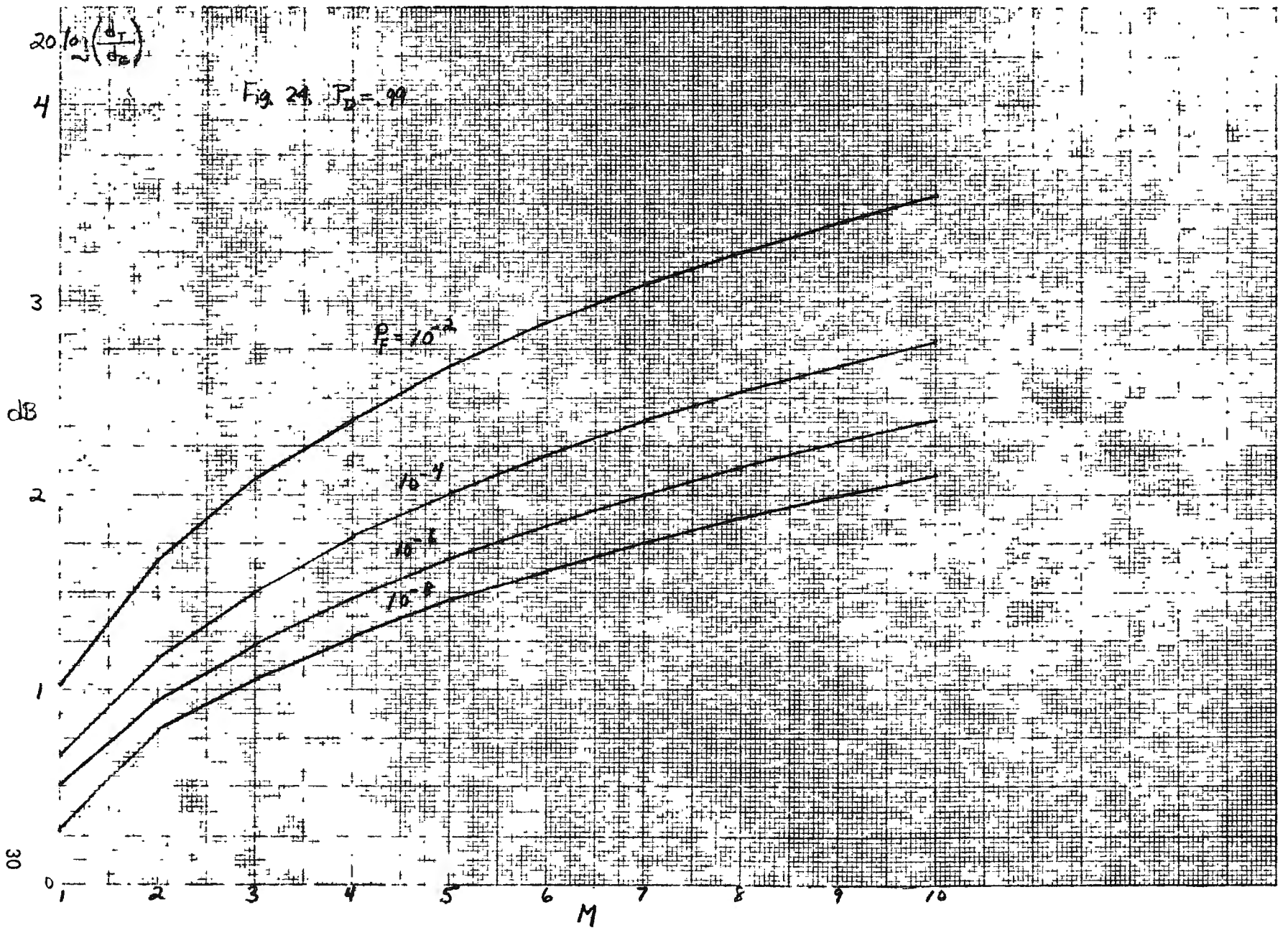

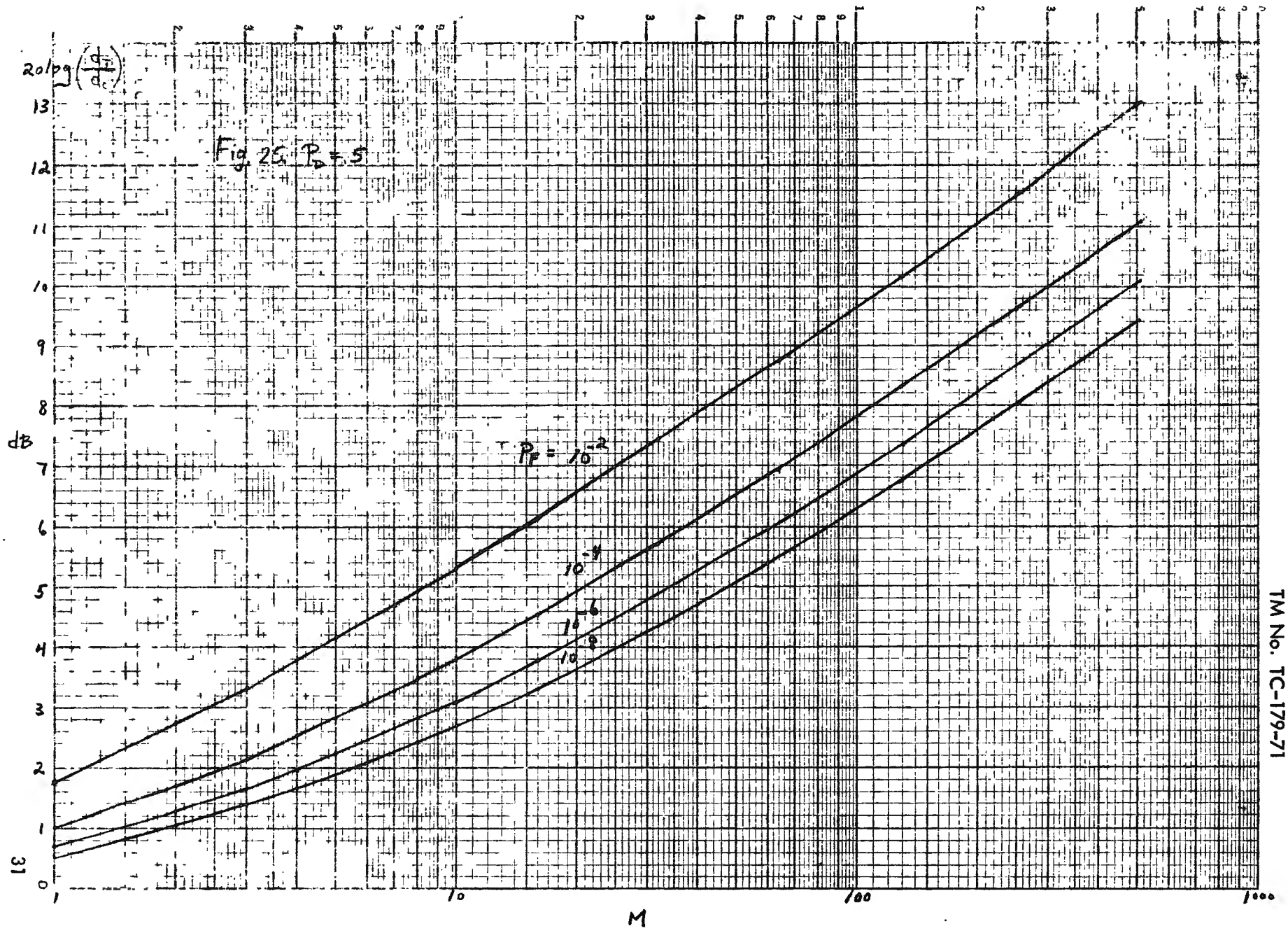
Fig 25 $P_D = .5$
$20 \log\left(\frac{q}{q_c}\right)$
dB
$P_F = 10^{-2}$
10^{-4}
10^{-6}
10^{-8}
M
1
10
100
1000

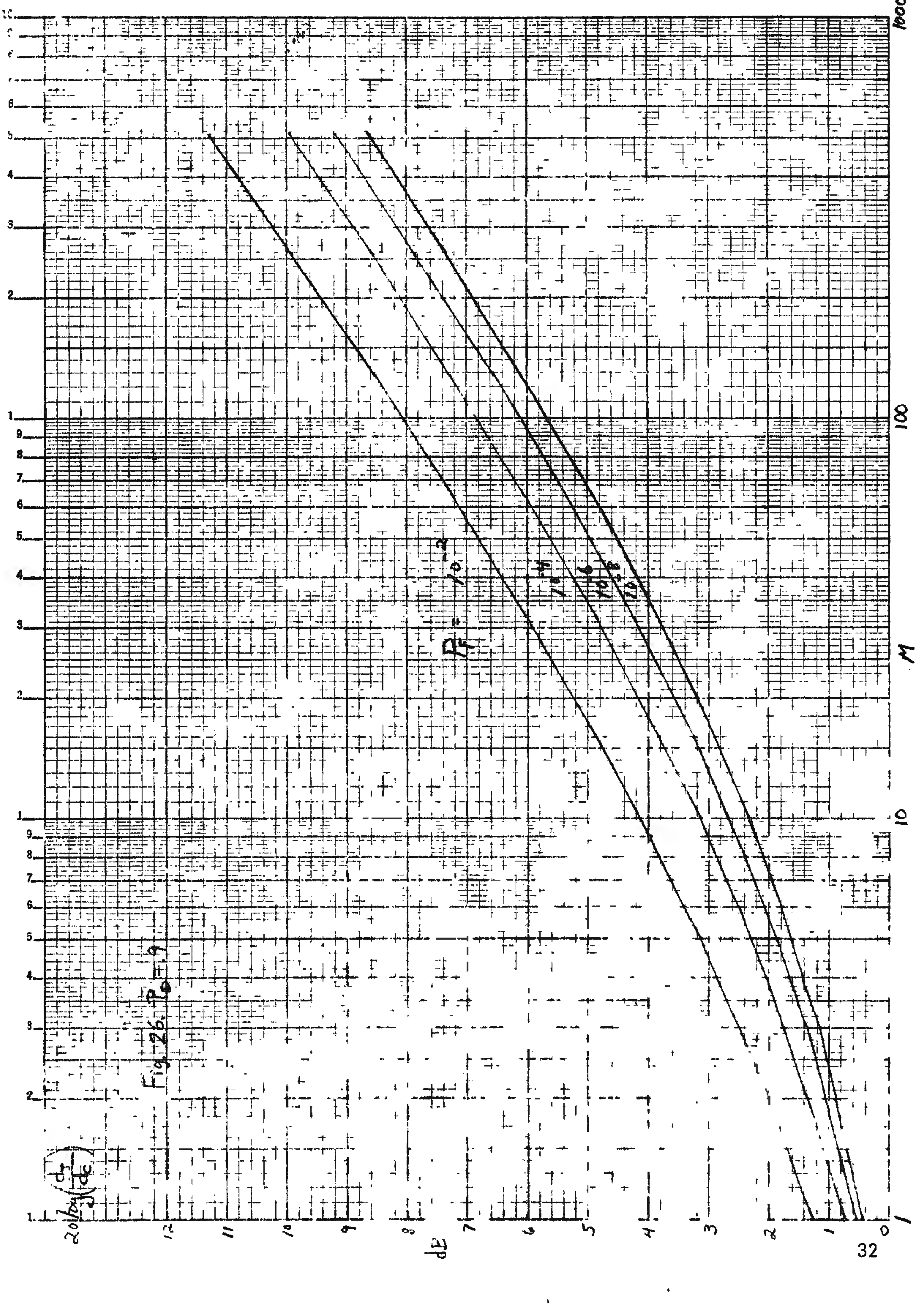
Fig 26. P_D = .9
P_F = 10^-2
10^-4
10^-6
10^-8
M
dB
20 log (d_J/d_c)
1000
100
10
1

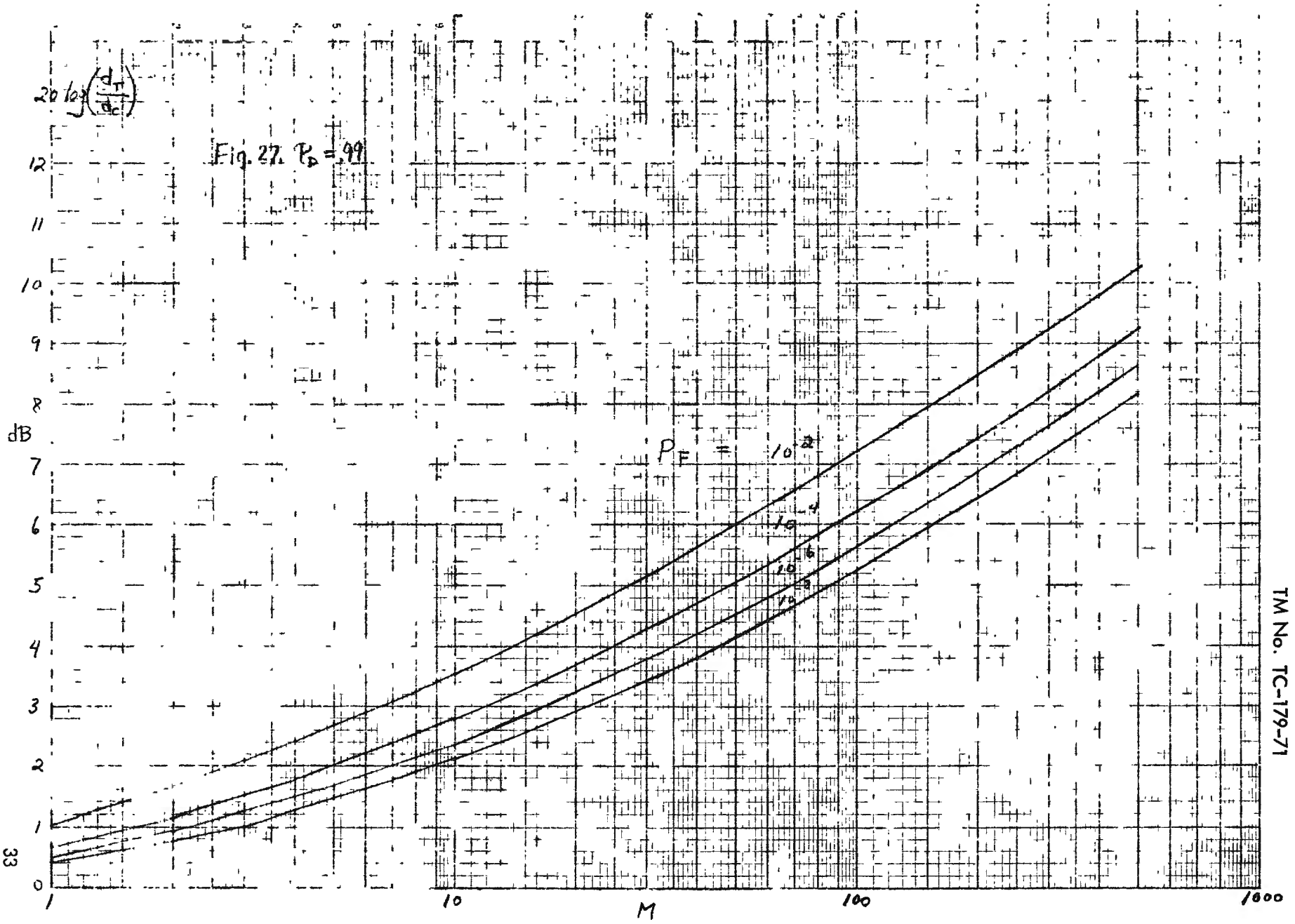
$20 \log\left(\frac{d_T}{d_c}\right)$
Fig. 27. $P_D = .99$
dB
$P_F = 10^{-2}$
10^{-4}
10^{-6}
10^{-8}
M
1
10
100
1000

APPENDIX A

PHASE-COHERENT DETECTION (PCD)

Consider the linear filter depicted in Fig. A1. Input process $x(t)$ is

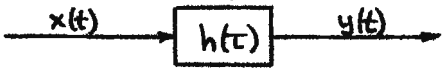

Fig. A1. Linear Filter

observed for $a < t < b$, and passed through filter h. The input is given by

$$x(t) = \left\{ \begin{array}{c} n(t) \\ \text{OR} \\ s(t)+n(t) \end{array} \right\}. \tag{A1}$$

Noise $n(t)$ is zero-mean stationary Gaussian, with correlation $R_n(\tau)$, and double-sided power spectrum $G_n(f)$. Signal $s(t)$ is deterministic, with voltage density spectrum $S(f)$. We have

$$y(t) = y_s(t) + y_n(t), \tag{A2}$$

where

$$y_s(t) = \int_a^b d\tau\, h(t-\tau)\, s(\tau),$$

$$y_n(t) = \int_a^b d\tau\, h(t-\tau)\, n(\tau). \tag{A3}$$

Suppose we sample output $y(t)$ at time T (which is arbitrary), and compare $y(T)$ with a threshold L for purposes of signal detection:

$$z \equiv y(T) \gtrless L. \tag{A4}$$

Random variable (RV) z is Gaussian, with

$$E\{z\} = \left\{ \begin{array}{c} 0 \\ \text{OR} \\ y_s(T) \end{array} \right\} \equiv \left\{ \begin{array}{c} 0 \\ \text{OR} \\ m \end{array} \right\}, \tag{A5}$$

and

$$\text{Var}\{z\} = \int_a^b\int_a^b d\tau_1\, d\tau_2\, h(T-\tau_1)\, h(T-\tau_2)\, R_n(\tau_1-\tau_2) \equiv \sigma^2. \tag{A6}$$

The probability density function (PDF) of z for signal present is

$$p_1(z) = (2\pi)^{-1/2}\,\sigma^{-1}\,\exp\left[-\tfrac{1}{2}\left(\frac{z-m}{\sigma}\right)^2\right]. \tag{A7}$$

The probability of detection is then

$$P_D = \int_L^\infty dz\, p_1(z) = \Phi\left(\frac{m}{\sigma} - \Lambda\right), \tag{A8}$$

where normalized threshold

$$\Lambda \equiv L/\sigma, \tag{A9}$$

and

$$\Phi(x) \equiv \int_{-\infty}^{x} dt\,(2\pi)^{-1/2}\exp(-t^2/2). \tag{A10}$$

The probability of false alarm is obtained by setting $m=0$ in (A8):

$$P_F = \Phi(-\Lambda). \tag{A11}$$

Now define

$$d_c = \frac{m}{\sigma} = \frac{\text{mean of filter output}}{\text{standard deviation of filter output}} = \frac{\int_a^b d\tau\, h(T-\tau)\,s(\tau)}{\left[\int_a^b\int_a^b d\tau_1 d\tau_2\, h(T-\tau_1)h(T-\tau_2)R_n(\tau_1-\tau_2)\right]^{1/2}} \tag{A12}$$

Then

$$P_F = \Phi(-\Lambda),\quad P_D = \Phi(d_c - \Lambda). \tag{A13}$$

Λ can be chosen for a desired P_F (Ref. 4, Tables 26.5 and 26.6); the actual P_D depends additionally on d_c. Curves of performance are given in Ref. 1, Figs. IV.1 and IV.2.

Letting $u = z/\sigma$ in (A7), the PDFs for signal present and absent are, respectively

$$p_1(u) = (2\pi)^{-1/2}\exp\left[-\tfrac{1}{2}(u-d_c)^2\right],$$
$$p_0(u) = (2\pi)^{-1/2}\exp\left[-\tfrac{1}{2}u^2\right], \tag{A14}$$

and depend only on the parameter d_c. Thus the receiver operating characteristics (ROC) depend only on d_c.

Equations (A12) and (A13) are the most general situation; filter h is arbitrary. We can investigate loss of performance due to wrong sampling instant T, or lack of knowledge of s or R_n, or any realization of filter h. (d_c^2 could be called the filter output power-SNR, but it is not necessary).

Several specializations of the general results above are possible; they are considered below.

Case 1 Optimum filter

Choose h such that d_c is maximized. It is the solution h_1 of the integral equation

$$\int_a^b d\tau\, h_1(T-\tau) R_n(t-\tau) = s(t), \quad a < t < b. \tag{A15}$$

The maximum value of d_c is then d_{c_1}, where

$$d_{c_1}^2 = \int_a^b d\tau\, h_1(T-\tau)\, s(\tau). \tag{A16}$$

Case 2 Optimum filter; Infinite Observation Interval; General Noise Spectrum

As $a \to -\infty$, $b \to +\infty$, the integral equation (A15) has the solution

$$H_2(f) = \frac{S^*(f) \exp(-i 2\pi f T)}{G_n(f)}, \tag{A17}$$

and the maximum d_c is d_{c_2}, where

$$d_{c_2}^2 = \int_{-\infty}^{\infty} df\, \frac{|S(f)|^2}{G_n(f)}. \tag{A18}$$

Case 3 Optimum filter; Finite Observation Interval; White Noise

For white noise, but finite observation interval,

$$G_n(f) = N_d, \text{ all } f \text{ (double-sided spectrum)}, \tag{A19}$$

$$R_n(\tau) = N_d\, \delta(\tau),$$

and the integral equation (A15) has the solution

$$h_3(T-\tau) = \frac{1}{N_d} s(\tau), \quad a < \tau < b, \tag{A20}$$

with a maximum d_c of d_{c_3}:

$$d_{c_3}^2 = \frac{1}{N_d} \int_a^b dt\, s^2(t) = \frac{E_{ab}}{N_d} , \tag{A21}$$

where E_{ab} is the received signal energy in (a, b).

Case 4 Optimum Filter; Infinite Observation Interval; White Noise

The maximum value of d_c is d_{c_4}, where

$$E_{ab} = E;\ h_4(T-\tau) = \frac{1}{N_d}\, s(\tau),\ \text{all } \tau;\ d_{c_4}^2 = \frac{E}{N_d} ; \tag{A22}$$

and E is the total received signal energy over all time.

APPENDIX B

PHASE-INCOHERENT DETECTION (PID)

The processor of interest here is depicted in Fig. B1. Input process $x(t)$

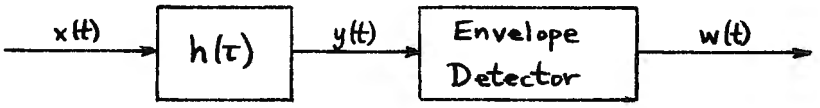

Figure B1. Linear Filter and Envelope Detector

is observed for $t \in (a,b)$, and passed through filter h. The input is given by

$$x(t) = \left\{ \begin{array}{c} n(t) \\ \text{OR} \\ s(t)+n(t) \end{array} \right\}. \tag{B1}$$

Noise $n(t)$ is zero-mean stationary Gaussian, with narrow-band spectrum G_n.
Signal $s(t)$ is deterministic except for unknown phase, and narrow-band.
Filter $h(\tau)$ is narrow-band.

Let*

$$\begin{aligned} s(t) &= \mathrm{Re}\left\{ \underline{s}(t) \exp\left(i 2\pi f_o t + i\theta\right)\right\}, \\ n(t) &= \mathrm{Re}\left\{ \underline{n}(t) \exp(i 2\pi f_o t)\right\}, \\ h(\tau) &= \mathrm{Re}\left\{ \underline{h}(\tau) \exp(i 2\pi f_o \tau)\right\}, \\ y(t) &= \mathrm{Re}\left\{ \underline{y}(t) \exp(i 2\pi f_o t)\right\}. \end{aligned} \tag{B2}$$

RV θ is uniformly distributed over 2π. The same center frequency f_o is no restriction, as the complex envelopes (underlined quantities in (B2)) can absorb differences in center frequencies. The complex envelope of $y(t)$ is

*Complex notation is used freely in this Appendix; see Ref. 1, Ch. 2, for example.

$$\underline{y}(t) = \frac{1}{2}\int_a^b d\tau\, \underline{h}(t-\tau)\left[\underline{s}(\tau)\, e^{i\theta} + \underline{n}(\tau)\right] \equiv \underline{y}_s(t) + \underline{y}_n(t), \text{ if signal present.} \tag{B3}$$

The output of Fig. B1 is given by

$$w(t) = \left|\underline{y}(t)\right|. \tag{B4}$$

Suppose we sample $w(t)$ at time T (arbitrary), and compare with a threshold L for purposes of signal detection:

$$z \equiv w(T) \gtrless L. \tag{B5}$$

Then using (B4) and (B3),

$$z = \left|\underline{y}_s(T) + \underline{y}_n(T)\right|. \tag{B6}$$

Let

$$\underline{y}_n(T) = x + iy. \tag{B7}$$

x and y are real Gaussian RVs, with

$$\overline{x} = \overline{y} = 0. \tag{B8}$$

And since (Ref. 1, Ch. 2)

$$\overline{\underline{y}_n^2(T)} = 0 = \overline{x^2} - \overline{y^2} + i2\overline{xy},$$

$$\overline{\left|\underline{y}_n(T)\right|^2} = \frac{1}{4}\iint_a^b d\tau_1\, d\tau_2\, \underline{h}(T-\tau_1)\underline{h}^*(T-\tau_2)R_{\underline{n}}(\tau_1-\tau_2) = \overline{x^2} + \overline{y^2}, \tag{B9}$$

there follows

$$\overline{xy} = 0,$$

$$\overline{x^2} = \overline{y^2} = \frac{1}{8}\iint_a^b d\tau_1\, d\tau_2\, \underline{h}(T-\tau_1)\underline{h}^*(T-\tau_2)R_{\underline{n}}(\tau_1-\tau_2) \equiv \sigma^2. \tag{B10}$$

Then

$$\overline{y_n^2(\tau)} = \tfrac{1}{2}\overline{|y_n(\tau)|^2} = \sigma^2. \tag{B11}$$

Let

$$y_s(\tau) = R + iI \quad \text{for fixed } \theta. \tag{B12}$$

Then using (B6), (B12), and (B7),

$$z = |R + iI + x + iy| = |A + iB| = \sqrt{A^2 + B^2}, \tag{B13}$$

where

$$A \equiv R + x, \quad B \equiv I + y. \tag{B14}$$

Then the PDF of real RVs A and B, for a given value of θ, is

$$p(A, B|\theta) = \frac{1}{2\pi\sigma^2} \exp\left[-\frac{(A-R)^2 + (B-I)^2}{2\sigma^2}\right]. \tag{B15}$$

The probability of detection for this given value of θ is

$$P_D(\theta) = \text{Prob}(z > L|\theta) = \iint_{\sqrt{A^2+B^2} > L} dA\, dB\; p(A, B|\theta). \tag{B16}$$

If we substitute (B15) in (B16) and let $A = r\cos\phi$, $B = r\sin\phi$,

$$P_D(\theta) = \int_{-\pi}^{\pi} d\phi \int_L^{\infty} dr\, r \frac{1}{2\pi\sigma^2} \exp\left[-\frac{r^2 - 2r(R\cos\phi + I\sin\phi) + R^2 + I^2}{2\sigma^2}\right]$$

$$= \int_L^{\infty} dr\, r \frac{1}{\sigma^2} \exp\left[-\frac{r^2 + |y_s(\tau)|^2}{2\sigma^2}\right] I_0\left(\frac{|y_s(\tau)|\, r}{\sigma^2}\right) =$$

$$= \int_{L/\sigma}^{\infty} du\, u \exp\left[-\tfrac{1}{2}u^2 - \tfrac{1}{2}\frac{|y_s(T)|^2}{\sigma^2}\right] I_0\left(\frac{|y_s(T)|}{\sigma}u\right) \equiv Q\left(\frac{|y_s(T)|}{\sigma}, \frac{L}{\sigma}\right), \tag{B17}$$

which is independent of θ. (This result is related to that in Helstrom, Ref. 1, p. 154, under (3,16), but is more general here because h is arbitrary).

Letting

$$\Lambda \equiv L/\sigma,$$

$$d_I \equiv \frac{|y_s(T)|}{\sigma} = \frac{\left|\int_a^b d\tau\, \underline{h}(T-\tau)\underline{s}(\tau)\right|}{\left[\frac{1}{2}\int_a^b\int_a^b d\tau_1 d\tau_2\, \underline{h}(T-\tau_1)\underline{h}^*(T-\tau_2)R_{\underline{n}}(\tau_1-\tau_2)\right]^{1/2}}, \tag{B18}$$

we have

$$P_D = Q(d_I, \Lambda),$$
$$P_F = Q(0, \Lambda) = \exp(-\Lambda^2/2). \tag{B19}$$

Λ can be chosen for a desired P_F; the actual P_D depends additionally on d_I. Curves of performance are given in Ref. 1, Figs. V.2 and V.3.

If we let $u = z/\sigma$ in (B13), it follows from (B14) - (B18) that the PDFs for signal present and absent are, respectively,

$$p_1(u) = u \exp\left[-\tfrac{1}{2}(u^2 + d_I^2)\right] I_0(d_I u),\ u > 0,$$
$$p_0(u) = u \exp\left[-\tfrac{1}{2}u^2\right],\ u > 0, \tag{B20}$$

and depend only on the parameter d_I. The quantity d_I has the following interpretation:

$$\frac{1}{2}d_I^2 = \frac{\frac{1}{2}|y_s(T)|^2}{\sigma^2} = \frac{\frac{1}{2}\mathcal{E}_{nv}^2\{y_s(t)\}\big|_{t=T}}{\overline{y_n^2(t)}\big|_{t=T}} =$$

$$= \frac{\text{instantaneous filter signal output power at time } T}{\text{instantaneous filter noise output power at time } T} . \quad \text{(B21)}$$

The denominator of (B21) is the ensemble average filter output noise power at time T. Steady state need not have been reached for either the signal or noise. $d_I^2/2$ could be called the instantaneous filter output power - SNR if desired; this is not necessary.

(As a special case of this general relation for d_I, consider a sine wave of amplitude A in the presence of noise, and an observation interval long enough for the filter output to reach steady state. Then

$$s(t) = A, \quad \text{(B22)}$$

and

$$y_s(\tau) = \frac{1}{2}\int_a^b d\tau\, h(\tau-\tau)A = \frac{1}{2} H(0)A \equiv P = \text{filter output sine-wave amplitude.} \quad \text{(B23)}$$

The filter output noise power is

$$\overline{y_n^2(t)} = \sigma^2. \quad \text{(B24)}$$

Then

$$\frac{d_I^2}{2} = \frac{\frac{1}{2}P^2}{\sigma^2} = \text{filter output power-SNR.} \quad \text{(B25)}$$

Several specializations of the general results (B18) and (B19) now follow:

Case 1 Optimum Filter

Choose h such that d_I is maximized. It is the solution h_1 of the integral equation

$$\int_a^b d\tau\, h_1^*(\tau-\tau)R_s(t-\tau) = s(t), \quad a<t<b. \quad \text{(B26)}$$

The maximum value of d_I is then d_{I_1}, where

$$d_{I_1}^2 = 2\int_a^b d\tau\, h_1(\tau-\tau)s(\tau), \quad \text{(B27)}$$

(which is always real and non-negative). The reason this result for $d_{I_1}^2$ differs from Helstrom, Ref. 1, p. 151, (3.6) by a factor of 2 is due to a different definition of R_n. Looking at Helstrom, Ch. II, sect. 5, we find his $\tilde{\phi}(\tau) = \frac{1}{2} R_n(\tau)$. Therefore, p. 147, (2.16) gives $Q(\tau) = 2\underline{h}_1^*(T-\tau)$, and his (3.6), p. 151 becomes identical to our $d_{I_1}^2$.

Case 2 Optimum Filter; Infinite Observation Interval; General Noise Spectrum

As $a \to -\infty$, $b \to +\infty$, the integral equation (B26) has the solution

$$\underline{H}_2(f) = \frac{\underline{S}^*(f) \exp(-i2\pi f T)}{G_n(f)}, \tag{B28}$$

and the maximum d_I is d_{I_2}, where

$$d_{I_2}^2 = 2\int_{-\infty}^{\infty} df \, \frac{|\underline{S}(f)|^2}{G_n(f)}. \tag{B29}$$

Case 3 Optimum Filter; Finite Observation Interval; White Noise

For white noise, but finite observation interval,

$$\begin{aligned} G_n(f) &= N_d, \quad \text{all } f, \\ G_n(f) &= 4N_d, \quad \text{all } f, \\ R_n(\tau) &= 4N_d \delta(\tau), \end{aligned} \tag{B30}$$

and the integral equation (B26) has the solution

$$\underline{h}_3(T-\tau) = \frac{1}{4} \frac{\underline{S}^*(\tau)}{N_d}, \quad a < \tau < b, \tag{B31}$$

with a maximum d_I of d_{I_3}:

$$d_{I_3}^2 = \frac{1}{2N_d} \int_a^b d\tau \, |\underline{s}(\tau)|^2 = \frac{E_{ab}}{N_d}, \tag{B32}$$

where E_{ab} is the received signal energy in (a,b). This relation for d_{I_3}, combined with $p_1(u)$ in (B20), agrees with Davies, Ref. 5 (remember that $N_o = 2N_d$).

Case 4 Optimum Filter; Infinite Observation Interval; White Noise

The maximum value of d_I is d_{I_4}, where

$$E_{ab} = E,$$
$$\underline{h}_4(T-\tau) = \frac{1}{4}\,\frac{\underline{s}^*(\tau)}{N_d}, \text{ all } \tau, \tag{B33}$$
$$d_{I_4}^2 = E/N_d,$$

and E is the total received signal energy over all time.

Notice from (A21), (A22), (B32), and (B33) that

$$d_{c_3} = d_{I_3}, \quad d_{c_4} = d_{I_4} \tag{B34}$$

for the same signal waveform and noise spectrum. These are special cases of the more general relation

$$d_{c_1} = d_{I_1}, \tag{B35}$$

which holds for narrow-band signals and noise. To see this, let

$$\underline{s}(t) = \mathrm{Re}\left\{\underline{\hat{s}}(t)\exp(i2\pi f_0 t)\right\},$$
$$h_1(\tau) = \mathrm{Re}\left\{\underline{\hat{h}}(\tau)\exp(i2\pi f_0\tau)\right\}, \tag{B36}$$
$$R_n(\tau) = \tfrac{1}{2}\mathrm{Re}\left\{R_{\underline{n}}(\tau)\exp(i2\pi f_0\tau)\right\} \quad (\text{using (B2)}),$$

in Case 1 of PCD, Appendix A. Using the high-frequency behavior of $\exp(i2\pi f_0 t)$, the integral equation in PCD, Case 1, becomes

$$\int_a^b d\tau\, \frac{1}{4}\,\underline{\hat{h}}^*(T-\tau)\,e^{-i2\pi f_0 T} R_{\underline{n}}(t-\tau) = \underline{\hat{s}}(t), \quad a<t<b. \tag{B37}$$

Defining

$$\tilde{\underline{h}}(T-\tau) = \frac{1}{4}\hat{\underline{h}}(T-\tau)\, e^{i2\pi f_0 T}, \tag{B38}$$

this last integral equation becomes

$$\int_a^b d\tau\, \tilde{\underline{h}}^*(T-\tau) R_{\underline{s}}(t-\tau) = \underline{s}(t), \quad a < t < b. \tag{B39}$$

Then using the narrow-band behavior of s and h_1 again, $d_{c_1}^2$ becomes

$$\begin{aligned} d_{c_1}^2 &= \int_a^b d\tau\, \frac{1}{4}\hat{\underline{h}}(T-\tau) e^{i2\pi f_0 T}\, \underline{s}(\tau) + \text{complex conjugate} \\ &= \int_a^b d\tau\, \tilde{\underline{h}}(T-\tau)\, \underline{s}(\tau) + \text{complex conjugate} \\ &= 2\int_a^b d\tau\, \tilde{\underline{h}}(T-\tau)\, \underline{s}(\tau); \end{aligned} \tag{B40}$$

this is real (remember $\tilde{\underline{h}}$ is the solution of integral equation (B39)). But now (B39) and (B40) are identical to Case 1 of PCD, upon identifying

$$\tilde{\underline{h}}(T-\tau) = \underline{h}_1(T-\tau), \tag{B41}$$

or equivalently

$$\hat{\underline{h}}(T-\tau) = 4\,\underline{h}_1(T-\tau)\, e^{-i2\pi f_0 T}, \tag{B42}$$

or

$$\hat{\underline{h}}(\tau) = 4\,\underline{h}_1(\tau) e^{-i2\pi f_0 T}. \tag{B43}$$

Therefore

$$d_{c_1} = d_{I_1} \tag{B44}$$

for a given signal waveform and noise spectrum. Also, the optimum filters are identical except for an irrelevant phase in PID. (Scale factors are unimportant). See also Helstrom, Ref. 1, p. 154, for a similar statement.

However, it is not necessary that d_c equal d_I, as can be seen by sampling $y_s(t)$ in PCD at a zero of the high-frequency waveform; then $d_c = 0$ while $d_I \neq 0$. In fact, d_c can be negative, whereas $d_I \geq 0$ for all sampling instants.

Although $d_{c_1} = d_{I_1}$ for a given signal waveform and noise spectrum, performance is poorer for PID than for PCD, because the ROC for PID is governed by the Q-function, whereas the ROC for PCD is governed by the Φ -function.

Suppose instead, we want PCD and PID to yield the same performance, i.e., identical P_F, P_D. Then reading the corresponding ROCs, suppose we need values

$$\begin{aligned} d_{c_1} &= V_c \quad \text{for PCD,} \\ d_{I_1} &= V_I \ (> V_c) \quad \text{for PID.} \end{aligned} \tag{B45}$$

Then the increased SNR required by PID, in comparison to PCD, is, in dB,

$$20 \log_{10} (V_I / V_c). \tag{B46}$$

(The factor 20 is due to the fact that d is proportional to signal voltage, not power, in both PCD and PID).

APPENDIX C

PHASE-INCOHERENT DETECTION- M COMPONENTS (PID-M)

Input process $x(t)$ is observed for $t \in (a,b)$, where

$$x(t) = \left\{ \begin{array}{c} n(t) \\ \text{OR} \\ s(t)+n(t) \end{array} \right\}, \tag{C1}$$

where $s(t)$ and $n(t)$ are narrowband processes. Input signal $s(t)$ is composed of M components:

$$s(t) = \sum_{K=1}^{M} s_K(t),$$

where

$$s_K(t) = Re\left\{ \underline{s}_K(t) \exp(i2\pi f_0 t + i\theta_K) \right\}; \quad \underline{s}_K(t) = A_K F_K(t). \tag{C2}$$

A_K is the (real) amplitude of the K-th signal component; $\{F_K(t)\}_1^M$ all have equal amplitude. RVs $\{\theta_K\}_1^M$ are independent and uniformly distributed over a 2π interval.

Now consider the following processor:

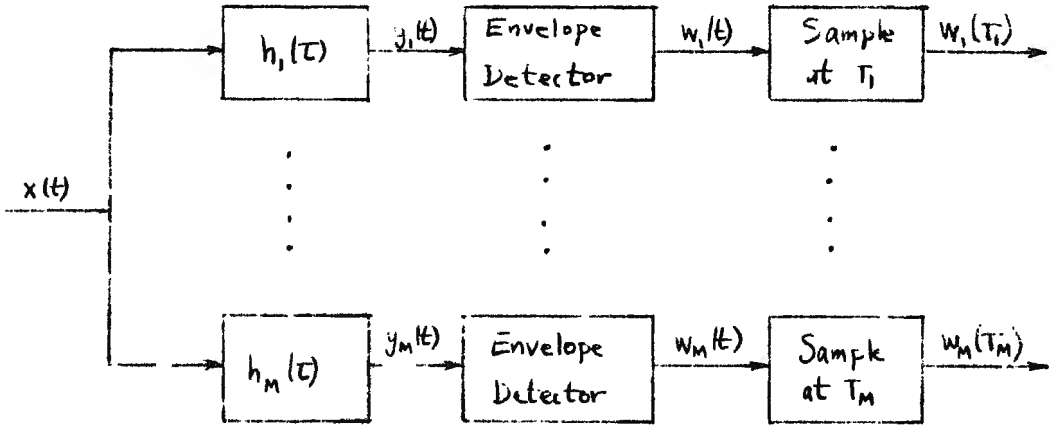

Figure C.1. Receiver Processor for M Components

The filters $\{h_j(\tau)\}$ are arbitrary for the moment. The complex envelope of $y_j(t)$ is

$$\underline{y}_j(t) = \tfrac{1}{2}\int_a^b d\tau\, \underline{h}_j(t-\tau)\left[\sum_{k=1}^{M} \underline{s}_k(\tau) e^{i\theta_k} + \underline{n}(\tau)\right]$$

$$= \sum_{k=1}^{M} e^{i\theta_k}\, \tfrac{1}{2}\int_a^b d\tau\, \underline{h}_j(t-\tau)\, \underline{s}_k(\tau) \qquad \text{(C3)}$$

$$+ \tfrac{1}{2}\int_a^b d\tau\, \underline{h}_j(t-\tau)\, \underline{n}(\tau).$$

We sample $w_j(t)$ at time T_j . The signal component of $\underline{y}_j(T_j)$ is, for given $\{\theta_k\}$,

$$\sum_{k=1}^{M} e^{i\theta_k}\, \tfrac{1}{2}\int_a^b d\tau\, \underline{h}_j(T_j-\tau)\, \underline{s}_k(\tau). \qquad \text{(C4)}$$

We shall assume that

$$\int_a^b d\tau\, \underline{h}_j(T_j-\tau)\, \underline{s}_k(\tau) = A_k \int_a^b d\tau\, \underline{h}_j(T_j-\tau) F_k(\tau) = 0 \quad \text{if } j \neq k. \qquad \text{(C5)}$$

This means that the j-th branch of the processor does not respond at time T_j to the K-th input signal component if $j \neq K$. This occurs, for example, if the signal components are disjoint with each other in time and/or frequency and if each filter is approximately matched to its corresponding signal; this is a realistic situation. The signal component of $\underline{y}_j(T_j)$ is then

$$e^{i\theta_j}\, \tfrac{1}{2}\int_a^b d\tau\, \underline{h}_j(T_j-\tau)\, \underline{s}_j(\tau) \equiv C_j . \qquad \text{(C6)}$$

The noise component of $\underline{y}_j(T_j)$ is

$$\tfrac{1}{2}\int_a^b d\tau\, \underline{h}_j(T_j-\tau)\, \underline{n}(\tau) \equiv n_j . \qquad \text{(C7)}$$

This is a complex Gaussian RV with $\overline{n_j} = 0$, since $\overline{\underline{n}(t)} = 0$. Also

$$\overline{n_j n_k} = 0, \text{ since } \overline{\underline{n}(t_1)\underline{n}(t_2)} = 0.$$

And
$$\overline{n_j n_k^*} = \frac{1}{4}\int_a^b\int d\tau_1 d\tau_2\, \underline{h}_j(T_j-\tau_1)\underline{h}_k^*(T_k-\tau_2)R_{\underline{n}}(\tau_1-\tau_2)$$
$$= \frac{1}{4}\int_a^b\int d\tau_1 d\tau_2\, \underline{h}_j(T_j-\tau_1)\underline{h}_j^*(T_j-\tau_2)R_{\underline{n}}(\tau_1-\tau_2)\delta_{jk}, \tag{C8}$$

where we have used assumption (C5) above. Therefore, the noise components in $\{\underline{y}_j(T_j)\}_1^M$ are all independent.

The PDF of

$$w_j(T_j) = |\underline{y}_j(T_j)| = |C_j + n_j| \tag{C9}$$

is available from (B6)-(B20) as

$$p_1(w_j) = \frac{w_j}{\sigma_j^2}\exp\left[-\frac{1}{2}\frac{w_j^2}{\sigma_j^2} - \frac{1}{2}d_I^2(j)\right] I_0\left(d_I(j)\frac{w_j}{\sigma_j}\right),\ w_j \geq 0,$$
$$p_0(w_j) = \frac{w_j}{\sigma_j^2}\exp\left[-\frac{1}{2}\frac{w_j^2}{\sigma_j^2}\right],\ w_j \geq 0, \tag{C10}$$

where
$$\sigma_j^2 \equiv \frac{1}{2}\overline{|n_j|^2} = \frac{1}{8}\int_a^b\int d\tau_1 d\tau_2\, \underline{h}_j(T_j-\tau_1)\underline{h}_j^*(T_j-\tau_2)R_{\underline{n}}(\tau_1-\tau_2),$$
$$d_I(j) \equiv \frac{|C_j|}{\sigma_j} = \frac{\left|\int_a^b d\tau\, \underline{h}_j(T_j-\tau)\underline{s}_j(\tau)\right|}{\left[\frac{1}{2}\int_a^b\int d\tau_1 d\tau_2\, \underline{h}_j(T_j-\tau_1)\underline{h}_j^*(T_j-\tau_2)R_{\underline{n}}(\tau_1-\tau_2)\right]^{1/2}}. \tag{C11}$$

Due to the independence of the noise components in $\{\underline{y}_j(T_j)\}$, the likelihood ratio based on observations $\{w_j(T_j)\}_1^M$ is

$$\ell = \prod_{j=1}^M \exp\left[-\frac{1}{2}d_I^2(j)\right] I_0\left(d_I(j)\frac{w_j}{\sigma_j}\right)$$
$$= \exp\left[-\frac{1}{2}d_T^2\right]\sum_{j=1}^M \ln I_0\left(d_I(j)\frac{w_j}{\sigma_j}\right), \tag{C12}$$

where

$$d_T^2 \equiv \sum_{j=1}^{M} d_I^2(j) = \sum_{j=1}^{M} \frac{\left| \int_a^b d\tau\, h_j(\tau_j - \tau)\, \underline{s}_j(\tau) \right|^2}{\frac{1}{2}\int_a^b \int_a^b d\tau_1\, d\tau_2\, h_j(\tau_j - \tau_1) h_j^*(\tau_j - \tau_2) R_{\underline{n}}(\tau_1 - \tau_2)} \,. \tag{C13}$$

The optimum processor is therefore based upon a comparison of the RV

$$\sum_{j=1}^{M} \ln I_0\left(d_I(j) \frac{w_j}{\sigma_j} \right) \tag{C14}$$

with a threshold. But this processor requires knowledge of absolute signal levels for its realization.

We instead consider the sub-optimum processor (guided by (C14))

$$z = \sum_{j=1}^{M} w_j^2 \tag{C15}$$

and inquire into its exact performance. From the PDF $p_1(w_j)$ in (C10), the characteristic function (CF) of w_j^2 for signal present is

$$\left(1 - i2\sigma_j^2 \xi\right)^{-1} \exp\left[\frac{i\sigma_j^2 d_I^2(j) \xi}{1 - i2\sigma_j^2 \xi} \right]. \tag{C16}$$

At this point we will assume that all the σ_j^2 are equal. Recalling the definition of σ_j^2 in (C11), this is tantamount to assuming the noise has substantially the same spectral level in the region of each of the filters $\{h_j\}$. (The analysis could be extended to unequal $\{\sigma_j^2\}$; however, the computational effort would be significantly greater.) Denoting the common value by σ_I^2, the CF of z in (C15) is

$$\left(1 - i2\sigma_I^2 \xi\right)^{-M} \exp\left[\frac{i\sigma_I^2 d_T^2 \xi}{1 - i2\sigma_I^2 \xi} \right], \tag{C17}$$

which depends on $\{d_I(j)\}$ only through d_T as defined in (C13). The PDF of z is (Ref. 1, p. 174, (2.10) and (2.12)):

$$\frac{1}{2\sigma_I^2}\left(\frac{z}{d_T^2\sigma_I^2}\right)^{\frac{M-1}{2}} \exp\left[-\frac{1}{2}\frac{z}{\sigma_I^2} - \frac{1}{2}d_T^2\right] I_{M-1}\left(\frac{d_T\sqrt{z}}{\sigma_I}\right), \quad z \geq 0. \tag{C18}$$

Comparison of z with a threshold L yields (Ref. 1, p. 176)

$$P_D = \text{Prob}(z > L) = Q_M(d_T, \Lambda), \tag{C19}$$

where

$$\Lambda \equiv \frac{\sqrt{L}}{\sigma_I}, \tag{C20}$$

and

$$Q_M(\alpha, \beta) \equiv \int_\beta^\infty dx\, x\left(\frac{x}{\alpha}\right)^{M-1} \exp\left[-\frac{1}{2}x^2 - \frac{1}{2}\alpha^2\right] I_{M-1}(\alpha x). \tag{C21}$$

Also

$$P_F = Q_M(0, \Lambda) = \exp(-\Lambda^2/2)\sum_{j=0}^{M-1}\frac{(\Lambda^2/2)^j}{j!}. \tag{C22}$$

The performance of this suboptimum processor depends on the individual signal strengths only through the quantity (C13):

$$d_T^2 = \sum_{j=1}^{M} d_I^2(j). \tag{C23}$$

Thus it does not depend on how the signal energy is fractionalized into its individual components; d_T^2 alone counts. This holds even though the filters $\{h_j(\tau)\}_1^M$ in Fig. C1 are not matched to the received signal components.

The performance of the PID-M processor in Fig. C1 followed by a summation of squared outputs can be optimized by maximizing the quantity d_T. This in turn can be maximized by choosing filters $\{h_j(\tau)\}$ such that $\{d_I(j)\}$ are maximized. Let $\underline{h}_{1K}(t)$ be proportional to the optimum complex envelope for

the filter which maximizes $d_I(k)$ at time T_k when $s_k(t)+n_k(t)$ is received. Then from PID, Appendix B,

$$\int_a^b d\tau\, \underline{h}_{1k}^*(T_k-\tau)R_{\underline{n}}(t-\tau) = F_k(t),\ a<t<b. \tag{C24}$$

Notice that these filters do not require knowledge of the relative signal strengths of each component. The maximum $d_I(k)$ for each component is $d_{I_1}(k)$, where

$$d_{I_1}^2(k) = 2\int_a^b d\tau\, A\, \underline{h}_{1k}(T_k-\tau)\underline{s}_k(t) = A_k^2\, 2\int_a^b d\tau\, \underline{h}_{1k}(T_k-\tau)F_k(\tau), \tag{C25}$$

and we have used (C11), (C24), and (C2). The entry to P_D in (C19) is d_{T_1}, where

$$d_{T_1}^2 = \sum_{k=1}^{M} d_{I_1}^2(k). \tag{C26}$$

We do not have to assume infinite observation interval or white noise to reach these conclusions. The major assumptions are the disjoint signals (under (C5)) and the equal variances (under (C16)).

APPENDIX D

PHASE-COHERENT DETECTION-M COMPONENTS (PCD-M)

We limit consideration to the optimum receiving filter here; Appendix A covers the more general case. The phase-coherent detector collects all the signal energy of the M components and yields

$$P_D = \Phi(d_{c_1} - \lambda), \quad P_F = \Phi(-\lambda), \tag{D1}$$

where (from Appendix A),

$$d_{c_1}^2 = \int_a^b d\tau\, h_1(T-\tau)\, s(\tau), \tag{D2}$$

and h_1 is the solution of the integral equation

$$\int_a^b d\tau\, h_1(T-\tau) R_n(t-\tau) = s(t), \quad a < t < b. \tag{D3}$$

$s(t)$ is the total received signal, and T is the sampling instant (which is arbitrary).

Now, from (C2),

$$s(t) = \sum_{K=1}^{M} S_K(t) = \sum_{K=1}^{M} \mathrm{Re}\left\{A_K F_K(t) \exp(i2\pi f_0 t + i\theta_K)\right\}. \tag{D4}$$

Let

$$\int_a^b d\tau\, h_{1K}(T-\tau) R_n(t-\tau) = S_K(t), \quad a < t < b, \text{ for } 1 \le K \le M. \tag{D5}$$

Then the filter h_1 in (D3) is given by

$$h_1(T-\tau) = \sum_{K=1}^{M} h_{1K}(T-\tau). \tag{D6}$$

Also then

$$d_{c_1}^2 = \int_a^b d\tau\, h_1(T-\tau)\, s(\tau) = \int_a^b d\tau \sum_{k=1}^{M} h_{1k}(T-\tau) \sum_{j=1}^{M} s_j(\tau)$$

$$= \sum_{k=1}^{M} \sum_{j=1}^{M} \int_a^b d\tau\, h_{1k}(T-\tau)\, s_j(\tau). \tag{D7}$$

Now let us relate the $\{h_{1k}(\tau)\}$ of this section to the $\{\underline{h}_{1k}(\tau)\}$ in (C24). To this end, (using narrowband behavior of the optimum filter) let

$$h_{1k}(\tau) = \mathrm{Re}\left\{ \hat{\underline{h}}_{1k}(\tau) \exp(i 2\pi f_0 \tau) \right\}. \tag{D8}$$

Then (D5) becomes, using the narrow-band behavior of the various functions,

$$\int_a^b d\tau\, \frac{1}{4}\, \hat{\underline{h}}_{1k}^{*}(T-\tau) R_{\underline{n}}(t-\tau) e^{-i 2\pi f_0 T} = A_k F_k(t) e^{i\theta_k}, \quad a < t < b. \tag{D9}$$

Comparing this with (C24), we see that

$$\frac{1}{4}\, \hat{\underline{h}}_{1k}(T-\tau) e^{i 2\pi f_0 T} = A_k e^{-i\theta_k} \underline{h}_{1k}(T_k-\tau), \quad a < \tau < b. \tag{D10}$$

Thus, the k-th phase-coherent filter $\hat{\underline{h}}_{1k}$ requires knowledge and use of θ_k, whereas the phase-incoherent filter $\underline{h}_{1k}$ does not. Then there follows

$$\int_a^b d\tau\, h_{1k}(T-\tau)\, s_j(\tau) = \int_a^b d\tau\, \frac{1}{2}\left\{ \hat{\underline{h}}_{1k}(T-\tau) e^{i 2\pi f_0 (T-\tau)} + \hat{\underline{h}}_{1k}^{*}(T-\tau) e^{-i 2\pi f_0 (T-\tau)} \right\} \cdot$$

$$\frac{1}{2}\left\{ A_j F_j(\tau) e^{i\theta_j} e^{i 2\pi f_0 \tau} + A_j F_j^{*}(\tau) e^{-i\theta_j} e^{-i 2\pi f_0 \tau} \right\}$$

$$= \frac{1}{4} \int_a^b d\tau\, \hat{\underline{h}}_{1k}(T-\tau) e^{i 2\pi f_0 T} A_j F_j(\tau) e^{i\theta_j} + \text{complex conjugate} \tag{D11}$$

$$= \int_a^b d\tau\, A_k e^{-i\theta_k} \underline{h}_{1k}(T_k-\tau) A_j F_j(\tau) e^{i\theta_j} + \text{complex conjugate} \tag{D12}$$

$$= A_k^2 \int_a^b d\tau \; \underline{h}_{ik}(T_k - \tau) F_k(\tau) \delta_{jk} + \text{complex conjugate} \tag{D13}$$

$$= d_{I_1}^2(k)\, \delta_{jk} \, . \tag{D14}$$

The transition to (D11) utilizes the high-frequency character of $\exp(i2\pi\xi_0 t)$, (D12) utilizes (D10), (D13) utilizes (C5), and (D14) utilizes (C25). Then from (D7) and (C26),

$$d_{c_1}^2 = \sum_{k=1}^{M} d_{I_1}^2(k) = d_{T_1}^2 \, . \tag{D15}$$

Therefore

$$d_{c_1} = d_{T_1} \, . \tag{D16}$$

That is, for a <u>given</u> signal waveform and noise statistics, $d_{c_1} = d_{T_1}$ under the assumptions above. However, the ROC for PID-M is poorer than the ROC for PCD-M, because the former is governed by the Q_M-function, whereas the latter is governed by the Φ-function.

If PID-M and PCD-M are to yield the <u>same</u> P_D, P_F, suppose we need values

$$\begin{aligned} d_{c_1} &= V_c \text{ for PCD-M,} \\ d_{T_1} &= V_I \; (>V_c) \text{ for PID-M.} \end{aligned} \tag{D17}$$

Then since each "d" is proportional to signal voltage (not power), the increased SNR required by the PID-M is, in dB,

$$20 \log_{10} (V_I / V_c). \tag{D18}$$

APPENDIX E

GAUSSIAN APPROXIMATION

The CF of decision variable z in (C15) is given by (C17). The CF of the normalized variable $u = z/\sigma_I^2$ is then

$$\left(1-i2\varphi\right)^{-M} \exp\left[\frac{i d_T^2 \varphi}{1-i2\varphi}\right]. \tag{E1}$$

For large M, only small values of φ lead to significant values of the CF (E1). Then since

$$1-i2\varphi \cong \exp\left(-i2\varphi+2\varphi^2\right) \quad \text{to order } \varphi^2, \tag{E2}$$

and

$$\exp\left[\frac{i d_T^2 \varphi}{1-i2\varphi}\right] \cong \exp\left[i\varphi\left(1+i2\varphi\right)d_T^2\right] \quad \text{to order } \varphi^2, \tag{E3}$$

(E1) becomes

$$\exp\left[i\varphi\left(d_T^2+2M\right) - 2\varphi^2\left(d_T^2+M\right)\right] \quad \text{to order } \varphi^2. \tag{E4}$$

The PDF corresponding to CF (E4) is

$$p(x) = \frac{1}{\sqrt{2\pi}\,2\sqrt{d_T^2+M}} \exp\left[-\frac{1}{2}\frac{\left(x-d_T^2-2M\right)^2}{4\left(d_T^2+M\right)}\right], \tag{E5}$$

which is a Gaussian RV with mean d_T^2+2M and variance $4\left(d_T^2+M\right)$.

(E5) is consistent with considering the RV

$$u = \sum_{k=1}^{M} x_k^2 \tag{E6}$$

as a Gaussian RV. The statistics of $\{x_k^2\}_1^M$ are available upon consideration of (C15) and (C10); namely

$$\overline{x_k^2} = 2 + d_I^2(k), \quad \mathrm{Var}\{x_k^2\} = 4\left[1 + d_I^2(k)\right]. \tag{E7}$$

There follows immediately from (E6), (E7), and (C13),

$$\bar{u} = 2M + d_T^2, \quad \mathrm{Var}\{u\} = 4\left(M + d_T^2\right). \tag{E8}$$

The probability of detection follows from (E5) as

$$P_D = \mathrm{Prob}(u > T) = \Phi\left(\frac{d_T^2 + 2M - T}{2\sqrt{d_T^2 + M}}\right), \tag{E9}$$

where T is a threshold, and Φ is given by (A10). The false-alarm probability is obtained by setting $d_T = 0$:

$$P_F = \Phi\left(\sqrt{M} - \frac{T}{2\sqrt{M}}\right). \tag{E10}$$

If we define a new threshold Λ according to

$$\sqrt{M} - \frac{T}{2\sqrt{M}} = -\Lambda, \tag{E11}$$

(E9) and (E10) become

$$P_F = \Phi(-\Lambda), \quad P_D = \Phi\left(\frac{d_T^2 - 2\sqrt{M}\Lambda}{2\sqrt{d_T^2 + M}}\right). \tag{E12}$$

Equation (E12) is plotted as crosses on Fig. 17. The new threshold Λ can be chosen for specified P_F.

REFERENCES

1. C. W. Helstrom, Statistical Theory of Signal Detection, Pergamon Press, N. Y., 1960

2. A. H. Nuttall, "Numerical Evaluation of Cumulative Probability Distribution Functions Directly from Characteristic Functions", NUSL Rpt. No. 1032, 11 Aug 1969. Also Proc. IEEE, Vol. 57, No. 11, pp. 2071-2072, Nov. 1969.

3. A. H. Nuttall, "Alternate Forms and Computational Considerations for Numerical Evaluation of Cumulative Probability Distributions Directly from Characteristic Functions", NUSC Rpt. No. NL-3012, 12 Aug 1970. Also Proc. IEEE, vol. 58, No. 11, pp. 1872-1873, Nov. 1970.

4. Handbook of Mathematical Functions, U. S. Dept of Comm., Nat. Bur. of Stds., Appl. Math. Series, No. 55, June 1964.

5. L. E. Davies, "Envelope Probability as a Function of E/N_o", Proc. IRE, vol.49, No. 5, pp. 971-972, May 1961.